Journal of Theoretical Biology

Modeling the Effects of Drugs of Abuse on Within-host Dynamics of Two HIV Species

--Manuscript Draft--

Manuscript Number:	JTB-D-22-00767R1
Article Type:	Regular paper
Keywords:	HIV; morphine; mutation; viral escape
Corresponding Author:	Naveen K. Vaidya San Diego State University San Diego, California UNITED STATES
First Author:	Peter Uhl
Order of Authors:	Peter Uhl
	Naveen Vaidya
Abstract:	Injection drug use is one of the most significant risk factors associated with contracting human immunodeficiency virus (HIV), and drug users infected with HIV suffer from a higher viral load and rapid disease progression. While replication of HIV may result in many mutant viruses that can escape recognition of the host's immune response, the presence of morphine (a drug of abuse) can decrease the viral mutation rate and cellular immune responses. This study develops a mathematical model to explore the effects of morphine-altered mutation and cellular immune response on the within-host dynamics of two HIV species, a wild-type and a mutant. Our model predicts that the morphine-altered mutation rate and cellular immune response allow the wild-type virus to out-compete the mutant virus, resulting in a higher set point viral load and lower CD4 count. We also compute the basic reproduction numbers and show that the dominant species is determined by morphine concentration, with the mutant dominating below and the wild-type dominating above a threshold. Furthermore, we identified three biologically relevant equilibria, the infection-free, mutant-only, and coexistence, which are completely characterized by fitness cost of mutation, mutant escape rate, and morphine concentration.
Suggested Reviewers:	Libin Rong libinrong@ufl.edu
	Dominik Wodarz dwodarz@uci.edu
	Elissa Schwartz ejs@wsu.edu
	Hana Dobrovolny h.dobrovolny@tcu.edu
	Jessica Conway jmc90@psu.edu

Department of Mathematics and Statistics
College of Sciences
San Diego State University
5500 Campanile Drive
San Diego CA 92182 · 7720
Tel: 619 · 594 · 6191
Fax: 619 · 594 · 6746
http://www.math.sdsu.edu

SAN DIEGO STATE UNIVERSITY

Naveen K. Vaidya, PhD
Professor of Mathematics
SDSU Disease Modeling Lab (SDSU-DiMoLab)
San Diego State University
E-mail: nvaidya@sdsu.edu Ph: 619-594-6697
Website: http://nvaidya.sdsu.edu/DiMoLab.html
http://nvaidya.sdsu.edu/

December 07, 2022

Dear Dr. Denise Kirschner
Co-Chief Editor, Journal of Theoretical Biology

We would like to thank you for the evaluation of our manuscript (Ms. No.: JTB-D-22-00767) and an opportunity to submit the revised version of the manuscript for publication in *Journal of Theoretical Biology*. We would also like to thank the reviewer for his/her helpful comments and constructive suggestions, which have helped improve our manuscript substantially. In the revised version of the paper, we have addressed/implemented all the comments and suggestions raised by the reviewer. A point-by-point response to the reviewer's comments is also included. Major revisions have been highlighted in red in the manuscript.

Thank you once again for your time and consideration, and we hope our revised manuscript is suitable for publication in *JTB*.

Sincerely,

Naveen K. Vaidya
Corresponding author (on behalf of all co-authors Peter Uhl and Naveen K. Vaidya)

Authors declare NO conflict of interst.

Response to the Reviewers' Comments

We thank the reviewer for careful reading of our manuscript and for providing constructive suggestions, which have substantially improved our manuscripts. All the comments/concerns have been addressed in the revised version of the manuscript. The major changes made are shown in red. The pointwise detailed responses to the reviewer's comments are given below.

Reviewer's Responses to Questions

*Note: In order to effectively convey your recommendations for improvement to the author(s), and help editors make well-informed and efficient decisions, we ask you to answer the following specific questions about the manuscript and provide additional suggestions where appropriate.

1. Are the objectives and the rationale of the study clearly stated?

Please provide suggestions to the author(s) on how to improve the clarity of the objectives and rationale of the study. Please number each suggestion so that author(s) can more easily respond.*

Reviewer #1: Yes

RESPONSE: Thank you.

Reviewer #2: Yes, the objectives and rationale are clearly stated.

RESPONSE: Thank you.

---

*2. If applicable, is the application/theory/method/study reported in sufficient detail to allow for its replicability and/or reproducibility?

Please provide suggestions to the author(s) on how to improve the replicability/reproducibility of their study. Please number each suggestion so that the author(s) can more easily respond.*

Reviewer #1: Mark as appropriate with an X:
Yes [X] No [] N/A []
Provide further comments here:

RESPONSE: Thank you.

Reviewer #2: Mark as appropriate with an X:
Yes [] No [X] N/A []
Provide further comments here:

Comment-1: *Section 3.1: In the LHS, what were taken as the lower and upper values of the range for each parameter? The authors mention "wider parameter sets" but this is insufficient.*

Response: We have now provided the lower and upper values of the range of each parameters used for LHS (Table 1).

Comment-2: *How were the PRCC values calculated? Did you use a program? Did you*

write your own code? If you wrote your own code based upon the method, please cite the paper.

Response: We used MATLAB functions to calculate PRCC of rank-transformed data as Pearson correlation coefficients between the vector of sampled parameters and model outputs (i.e., R_0^w, R_0^m, viral load, CD4+ counts). We have added additional writing to Section 3.1 explaining our process.

Comment-3: *Section 3.5: The LHS method is just a sampling method; it is not a method to detect sensitivity to parameters. Sensitivity is measured using PRCC analysis. The clarity of the writing in this section needs to be improved, because as is, it veers on being inaccurate.*

Response: We have rewritten Section 3.5 almost entirely as suggested by the reviewer. In the revised version, we have clearly explained the sampling procedure using LHS and sensitivity analysis using PRCC. We have also explained this clearly in section 3.1.

---

*3. If applicable, are statistical analyses, controls, sampling mechanism, and statistical reporting (e.g., P-values, CIs, effect sizes) appropriate and well described?

Please clearly indicate if the manuscript requires additional peer review by a statistician. Kindly provide suggestions to the author(s) on how to improve the statistical analyses, controls, sampling mechanism, or statistical reporting. Please number each suggestion so that the author(s) can more easily respond.*

Reviewer #1: Mark as appropriate with an X:
Yes [] No [] N/A [X]
Provide further comments here:

Response: Thank you.

Reviewer #2: Mark as appropriate with an X:
Yes [] No [X] N/A []
Provide further comments here:

Comment-1: *"Significant" is a word with a strict scientific meaning (p.10 and p.15). Use of this word necessitates a remark on the statistics that back the claim. Another word would perhaps be more appropriate here.*

Response: As suggested by the reviewer, we have replaced the word significant with other appropriate words (for example, substantial) throughout the manuscript.

---

4. Could the manuscript benefit from additional tables or figures, or from improving or removing (some of the) existing ones?

Please provide specific suggestions for improvements,

removals, or additions of figures or tables. Please number each suggestion so that author(s) can more easily respond.

Reviewer #1: No

Response: Thank you.

Reviewer #2: Yes, the manuscript would benefit from improving and removing existing figures.

Comment-1: *Figure 2: Label the units of the Morphine concentration (ug/l), on the x-axis on and in the figure caption's second sentence (i.e., M_thresh=54 ug/l). On the right, label the colorbar so the reader knows what changes as the color changes. Is this also M_thresh? The red line is misleading, pointing down at a 45 degree angle: B barely has an effect on the color past B=7 or so. It looks like it is almost just as easy to have a yellow region when B=10 as when B=50. Contrary to the figure caption, in this figure, M_thresh increases moving along nearly a vertical line, rather than the arrow from the upper left to lower right. Please correct.*

Response: We agree with the reviewer. We have now recreated the Figure 2 (Figure 3 in the revised version). As suggested, we have shown B varying only from 0 to 10 because M_{thresh} is most sensitive to changes in escape ratio *B* for low values only. We have labeled the colorbar, which indicated the value of M_{thresh}. The redline is removed as it creates confusion. We have also added the units for morphine on the left figure, and elsewhere in the manuscript.

Comment-2: *Fig 3a is difficult to interpret. Please explain.*

Response: In the revised manuscript, we have explained about Figure 4 (previous Figure 3) in details in Figure caption and in Section 3.3.3. Figure 4a is meant to demonstrate how we obtain the numerical value of V_m for the MOE. Each colored line in the figure represents a specific morphine concentration, and the x-intercept of each curve is the V_m value at the MOE for that concentration. Figure 4b shows the MOE V_m (i.e., x-intercepts of Figure 4a) for morphine concentration between 0 and 200 ug/l.

Comment-3: *Enlarge the font size in Fig 5cd as in Fig 5ab.*

Response: Font sizes are now consistent across all graphs of Figure 6 (previous Figure 5) and elsewhere in the manuscript.

Comment-4: *Fig 6: This figure is very interesting, but the results need to be normalized. If the VL starts out higher, then clearly it would take longer to reach 50, but does the % drop relative to the ss VL also lag? Please clarify.*

Response: We thank the reviewer for this excellent question. We have now added a subfigure in Figure 7 (previous Figure 6) with a normalized result. In the new subfigure, we simulated the viral dynamics until a steady state with M = 200. Once a steady state is

reached, we began ART under two conditions: one without morphine (M=0) and another with M = 200. These two conditions represent the first patient who stops taking drugs of abuse once ART begins and the second patient who continues taking drugs of abuse even after ART. The new result further confirms that the viral load falls below detection limit faster when morphine is not present. We have also explained this in Section 3.4.

Comment-5: *Fig 7 is hard to follow. Is M=0 on the left and M=200 on the right (just a guess)? If so, this should be indicated. However, PRCC values below 0.5 are not high enough to be indicative, so this figure is not meaningful and can be removed without any loss. Alternatively, include a discussion of what changes between one subfigure and the next (not simply listing the parameter names that are different, but discuss in terms of the mechanisms that the parameters represent and what this means for the results), why this is interesting, and relate it to morphine levels.*

Response: We decided to use the reviewer's alternative suggestion and rewrite Section 3.5 to include more interpretation of the PRCCs rather than simply reporting them. The revised manuscript emphasizes the difference in PRCCs between the presence ad absence of morphine for viral load and CD4+ counts. In particular, *F* and *B* have increased sensitivity for $M = 0$ because the mutant is the dominant strain. Each subfigure of Figure 8 (previous Figure 7) is now labeled to clearly show what each set of PRCCs are for. A detailed explanation is presented in Section 3.5

---

5. If applicable, are the interpretation of results and study conclusions supported by the data?

Please provide suggestions (if needed) to the author(s) on how to improve, tone down, or expand the study interpretations/conclusions. Please number each suggestion so that the author(s) can more easily respond.

Reviewer #1: Mark as appropriate with an X:
Yes [X] No [] N/A []
Provide further comments here:

Response: Thank you.

Reviewer #2: Mark as appropriate with an X:
Yes [] No [X] N/A []
Provide further comments here:

This is a very interesting idea and model on an extremely important and relevant topic! The model analysis is well-executed and addresses key questions, both mathematically and biologically. However, the main issue in this paper is not that the interpretation of the results is unsupported; it is simply the lack of interpretation of the model's results. Examples of this are present throughout the paper, some of which are listed below:

Response: We thank the reviewer for inspiring comments about our study (*very interesting idea and model on an extremely important and relevant topic! The model*

analysis is well-executed and addresses key questions, both mathematically and biologically.). We apologize for the lack of interpretation of the results in our previous manuscript. We have substantially changed our interpretation in the revised manuscript to describe them in a more meaningful way.

Comment-1*: What are the implications of the results? What does this study tell us that we didn't know before, that we can use going forward? It is clear that the authors' aim is to quantify the effects of opiate use on HIV infection, but what does this help us do - Does it give better treatment options? Does it shed light on behavior change (i.e., discourage drug use)?*

Response: While the effects of morphine in different aspects of viral dynamics have been documented in experiments, the degree in which those effects are translated in viral dynamics are not known before. This is the first model which considers all three effects in the context of viral fitness, immune escape, and morphine level, and provide quantitative knowledge on those effects previously not known. For example, the morphine level altering the dominant viral species, quantitative hindrance effect of morphine on treatment efficacy are some of the most significant results that were not known before. These results provide useful information for better treatment options and behavioral change. The model also motivates further experimental study into the effect of drug use on viral mutation. In the revised manuscript, we have discussed these implications of results in the conclusion section.

Comment-2*: Figure 1 is delivered with no explanation of results, implications, or useful conclusions. The results state that certain parameters (given by parameter name only) correlate with the R naughts, but not what that indicates or why that is interesting/relevant. The results need to be interpreted (throughout the paper), not just reported. Do the results make sense given previous knowledge? Are they consistent with what would be expected, or are they unexpected, and why? How do they relate to the biology being modeled?*

Response: The part of Section 3.3.1 discussing sensitivity to parameters has been extensively rewritten. The revised manuscript provides details about the effects of *F* and *B* on R_0^w and R_0^m and other mechanisms, rather than simply reporting the values.

Comment-3: *Why are the local sensitivity indices and the prcc results so different in magnitude? Why are both measures of sensitivity needed? Is the point here to compare the methods to one another, and if so, what does the comparison reveal? What is the interpretation that of the finding that Rm0 is positively related to B and negatively related to F, and what does this mean in terms of the meanings of these thresholds and parameters? The key sentences that tie the results together with the questions that the authors set out to answer are absent.*

Response: The purpose of both sensitivity analyses is to determine which parameters have the largest effect on the model output; the local sensitivity provides the instantaneous change expected at the basic parameters (estimated using experimental

data previously) while the PRCC in LHS techniques provides expected change in global parameter range. Having local and global analysis strengthens our conclusion about which parameters are most important and can inform experimental work. The sensitivities of *F* and *B* on the mutant reproduction number reflect that the mutant benefits from low fitness cost of mutation and high escape rate from immune response. This and other interpretations are discussed in the rewritten section 3.1.

Comment: *4. What is the interpretation of the finding that morphine affects the long-term dynamics in terms of which species, if any, survive, given different values of the mutant fitness and the propensity for the mutant to escape from the CTLs? What does the model conclude about the short and long-term outcome of an HIV infection in the presence of morphine that we did not already know from clinical data? What can be concluded about the characterization of stability of the equilibria - does lower B or higher F correspond with stability of an equilibrium and if so which one? Clearly state which equilibrium is stabilized by morphine. The M_thresh is interesting in terms of the dynamics, but why is it important - does this help contain the infection, stop progression, improve ART effectiveness? Should it be monitored for treatment or to reach a better outcome? Etc.*

Response: Section 3.3.5 and Figure 5 (previous Figure 4) characterize the stability of the three equilibria in terms of *M, F,* and *B*. High morphine tends to favor the wild-type virus and lead to the coexistence equilibrium, lower morphine can stabilize either the infection-free or mutant-only equilibria depending on the fitness of the mutant virus. One of the interesting results is the more fit wild-type virus dominates in the presence of morphine. M_thresh value provides the threshold for determining long-term outcome of the dynamics, which may help to predict infection outcome and to design ideal treatment protocols. None of such results has been documented as clinical data. We have added a summary paragraph to the end of Section 3.3.5 clearly stating these results.

The conclusion of section 3.3.3 is excellent because it says "This is expected because…" The other results need to be followed by this type of conclusion; otherwise the paper is unfinished.

Response: We thank the reviewer for stating that this conclusion is excellent. We have tried our best to present other results with such conclusions, including the ones which are model predicted that are either expected or unexpected. Even such model predicted unexpected or unknown results motivate further experiments.

---

6. Have the authors clearly emphasized the strengths of their study/theory/methods/argument?

Please provide suggestions to the author(s) on how to better emphasize the strengths of their study. Please number each suggestion so that the author(s) can more easily respond.

Reviewer #1: Yes

Response: Thank you.

Reviewer #2: Yes

Response: Thank you.

---

7. Have the authors clearly stated the limitations of their study/theory/methods/argument?

Please list the limitations that the author(s) need to add or emphasize. Please number each limitation so that author(s) can more easily respond.

Reviewer #1: Yes

Response: Thank you.

Reviewer #2: Yes

Response: Thank you.

---

8. Does the manuscript structure, flow or writing need improving (e.g., the addition of subheadings, shortening of text, reorganization of sections, or moving details from one section to another)?

Please provide suggestions to the author(s) on how to improve the manuscript structure and flow. Please number each suggestion so that author(s) can more easily respond.

Reviewer #1: No

Response: Thank you.

Reviewer #2: Yes, reorganization is needed.

Comment-1: *To improve the flow of the paper, Figure 5 should be Figure 1.*

Response: As suggested by the reviewer (comment-3 below), we tried to present analytical results first followed by the numerical results. Figure 6 (previous Figure 5) is a numerical result, so presenting it first would not appear to be in line with this strategy. Furthermore, Figures 7 and 8 (previous Figure 8 and 9) follow logically from Figure (previous Figure 5), so we feel that rearranging the order of these would disrupt the flow of the paper. That being said, we are happy to make these changes if the reviewer strongly feels that they are necessary.

Comment-2: *Rearrange the order of 3.3.3 and 3.3.2.*

Response: The order of Sections 3.3.3 and 3.3.2 have been rearranged. The order of Sections 3.3.1-3 is now Infection-free equilibrium, Wild-type only equilibrium, and Mutant-only equilibrium.

Comment: *3. The paper would flow better if first, the analytical results are provided, and then afterwards, the numerical results, as in most papers.*

Response: We have tried to arrange the manuscripts as suggested by the reviewer. The section relating to the basic reproduction numbers contains the main analytical results of the paper and is presented first, followed by analytical steady state analyses and then numerical results.

---

9. Could the manuscript benefit from language editing?

Reviewer #1: No

Response: Thank you.

Reviewer #2: No

Response: Thank you.

Further Comments/suggestions: *This field is optional. If you have any additional suggestions beyond those relevant to the questions above, please number and list them here.*

Reviewer #1: The manuscript describes a mathematical model that incorporates the effect of morphine on HIV infections. The authors use mathematical analysis, computer simulation, and sensitivity analysis to study the role of morphine in HIV infections. The manuscript is well-written and the analysis is thorough. I have a few minor comments:

Response: We thank the reviewer for finding our manuscript well-written and thorough analysis.

Comment-1: *I don't believe the authors need to change how mutation is incorporated in the model, but they could perhaps discuss/justify the following choices. Why is it assumed that there is a fitness "cost" (0<F<1) for mutations --- sometimes mutations result in a competitive advantage, particularly in the presence of drug treatment. Any thoughts on how a more competitive mutant might change the analysis? Why is there no back-mutation? Mutation in viruses is caused by random changes in the amino acid sequence --- surely it's just as likely to switch one way as it is to switch back?*

Response: Based on our experience on working with HIV viruses, the mutant viruses are usually less fit than wild-type virus (unlike in influenza virus, where some mutant virus gained competitive advantage). So, we considered a fitness "cost" (0<F<1) for mutations. We agree with the reviewer that the mutant virus may get net competitive advantage in the presence of antiretroviral therapy. But, this advantage is due to higher escape rate of mutant virus from drugs than its fitness cost. In this study too, the idea of net fitness is related to the fitness cost and immune escape ratio. Our rationale is that the mutant has an advantage over the wild-type by being able to escape from CTLs (the B parameter) and a disadvantage from the fitness cost of escape (F). The net difference in these two effects result in the net competitive advantage or disadvantage. Following the

curiosity of the reviewer, if we allow for an advantageous fitness cost (which could be modeled as a negative value for F), it will make much more likely that the mutant dominates the wild-type. Back-mutation was not included as effect of morphine on the back mutation is not known and we wanted to limit the number of terms (parameters) in the model. We have discussed these points, including our limitations in the revised manuscript.

Comment-2: *Units are sometimes italicized, sometimes not. This should be consistent.*

Response: Units are no longer italicized and are consistently throughout the revised manuscript.

Comment-3*: In the second point of the highlights, "outcome" should be "outcompete."*

Response: Thank you for pointing out this typo. We have made corrections.

Reviewer #2: This has the workings of a really excellent paper. The model is quite complex but it was clearly designed carefully. The mathematical analysis was carried out well, especially considering the effort involved given the number of parameters. The motivation for the numerics and figures shown is sound. However the study is incomplete because the results are not interpreted in light of the aims of the paper (as mentioned in 5.).

Response: We thank the reviewer for inspiring comments about our study (excellent paper, clearly designed model, well-carried analysis, and sound motivation for the numeric and figures). We apologize for the lack of interpretation of the results in our previous manuscript. We have substantially changed our interpretation in the revised manuscript to describe them in a more meaningful way.

Further improvements:

Comment-1: *Justify the first term of dC/dt. Why are the CTLs recruited at a constant rate? In the IFE, if there is no infection, then why is C*>0?*

Response: Assuming the production of CTL strictly proportional to infected cells may not be perfectly correct. Following the previous studies, we introduced a constant term ω in dC/dt equation to incorporate the potential background CTL production other than those proportional to infected cells or other uncertainties,. The case for the absence of such background production can be recovered by taking $\omega = 0$. Moreover, the constant term in the CTL equation allows us to create a non-zero steady-state for the infection-free equilibrium and allows us to generate interesting analytical results. We have explained this in the model description section and cited additional references that include this term when modeling CTLs in HIV infections.

Comment-2: *Was the MOE shown to be stable for M<M_thresh? Are all eigenvalues negative in their real parts? This work was hard to locate in the paper.*

Response: While we did not provide eigenvalues explicitly in the manuscript, we computed eigenvalues for morphine between 0 and 200 ug/l to determine stability for the MOE and CE. The real part of one eigenvalue of the MOE becomes positive as *M* increases through M_{thresh} and the CE becomes locally stable. This has been clarified in Section 3.3.3 of the revised manuscript.

Comment-3: *I could not find the section on the coexistence equilibrium. There is mention of the "three biological relevant equilibria," but after the IFE and MOE, the paragraph introducing the coexistence equilibrium was perhaps unintentionally deleted?*

Response: In the previous manuscript, we presented coexistence implicitly in the section on parameter spaces and stability. In that section we discussed conditions on morphine, fitness cost, and immune escape which stabilize the three equilibria. However, we agree with the reviewer that a section devoted to the coexistence equilibrium should be included for completeness. We have now added a subsection that discusses it and its stability.

Comment-4: *Since the model includes only 1 step of mutation and no back-mutation, use of the word "mutation" instead of "evolution" would be a bit more reasonable.*

Response: We agree with the reviewer and have changed the words accordingly.

Comment-5: *There many more modeling papers in the literature that look at a wild type strain, a mutant strain, and various factors that affect the dynamics. More of these should be cited. Where do the results of this study fall among the results of the many others?*

Response: This is a good point, and we have now added more citations, including additional HIV modeling studies that investigate wild-type/mutant dynamics. One of the references we cite is a model featuring viral mutation and cellular immune responses. An additional study investigating treatment optimization with a drug resistant mutant is also now discussed in the conclusion section.

Comment-6: *Adding a schematic diagram for the model would help. There may be such a diagram in Ref 35, but it is unclear if this paper is published yet (no date).*

Response: We appreciate this feedback and have added a schematic of the model as a new Figure (Figure 1).

Other comments/edits/typos:

Comment-1: *Some words like "a" or "the" are missing in several locations on page 16, and there is a noun/verb disagreement (boundary is, not are).*

Response: These typos have been corrected.

Comment-2: *Ref 35 is incomplete*

Response: We have complete information for Ref 35.

Comment-3: *Ref 39 - should it say post-operative? Why IV morphine in children rather than adults?*

Response: This has been corrected. We chose this reference because it includes intravenous blood-plasma concentration data relevant for our modeling.

Comment-4: *Section 2.2: 40980 cells/ml and 959020 cells/ml*

Response: This has been corrected.

Comment-5: *3.3.2: typo 'from' should be 'form'. Last line page 11.*

Response: This has been corrected.

Comment-6: *P.9: 'Sensitiveness' should be 'sensitivity'*

Response: This has been corrected.

Comment-7: *There should be stars in (13) since these equations have been set to 0 and are no longer varying.*

Response: This has been corrected.

Modeling the Effects of Drugs of Abuse on Within-host Dynamics of Two HIV Species

Peter M. Uhl[a,b,c], Naveen K. Vaidya[a,b,c,*]

[a] *Computational Science Research Center, San Diego State University, San Diego, CA, USA*
[b] *Department of Mathematics and Statistics, San Diego State University, San Diego, CA, USA*
[c] *Viral Information Institute, San Diego State University, San Diego, CA, USA*

Abstract

Injection drug use is one of the most significant risk factors associated with contracting human immunodeficiency virus (HIV), and drug users infected with HIV suffer from a higher viral load and rapid disease progression. While replication of HIV may result in many mutant viruses that can escape recognition of the host's immune response, the presence of morphine (a drug of abuse) can decrease the viral mutation rate and cellular immune responses. This study develops a mathematical model to explore the effects of morphine-altered mutation and cellular immune response on the within-host dynamics of two HIV species, a wild-type and a mutant. Our model predicts that the morphine-altered mutation rate and cellular immune response allow the wild-type virus to outcompete the mutant virus, resulting in a higher set point viral load and lower CD4 count. We also compute the basic reproduction numbers and show that the dominant species is determined by morphine concentration, with the mutant dominating below and the wild-type dominating above a threshold. Furthermore, we identified three biologically relevant equilibria, infection-free, mutant-only, and coexistence, which are completely characterized by the fitness cost of mutation, mutant escape rate, and morphine concentration.

Keywords: HIV, mutation, viral escape, morphine

*Corresponding author
5500 Campanile Dr
San Diego, Ca 92182
Email address: nvaidya@sdsu.edu (Naveen K. Vaidya)

1. Introduction

Human immunodeficiency virus (HIV) is a significant health concern worldwide, with 37.7 million infected people globally in 2021 [1]. In addition to sexual contact, HIV transmission is also commonly associated with recreational drug use through needle sharing between drug users [2, 3]. Drug use has also been shown to have several detrimental effects on people infected with HIV, such as a higher viral load, a more rapid progression to AIDS, a greater chance of HIV-related neurological complications, and an overall higher mortality rate [4, 5, 6, 7]. Therefore, it is essential to study how the conditioning of drugs of abuse affects the progression of HIV infections.

HIV replicates within target CD4+ T-cells. Individual virions bind to the target cell membrane, enter the target cell, replicate viral RNA, and then the infected cell releases the newly produced virus into the environment [8, 9, 10]. One of the defense mechanisms the host implements is a cellular immune response in the form of cytotoxic T-lymphocytes (CTLs), which are able to detect and kill infected cells by recognizing epitopes on the surface of infected cells, thereby limiting viral replication [11, 12]. The virus replication process is highly error-prone, resulting in many mutations [13]. Many mutant viruses express epitopes different from wild-type viruses and escape detection by CTLs [10, 13, 14]. Pressure to escape CTLs, combined with the high turnover of virions and infected cells, plays a significant role in allowing HIV to establish infection [15, 16, 17] and poses a major challenge in the control of the infection by immune responses, thereby causing obstacles in developing successful CTL-based vaccines [18, 19, 20].

Animal models with SIV (Simian Immunodeficiency Virus) in rhesus macaques have demonstrated several adverse effects that drugs of abuse can have on the prognosis of infection. In the experiment by Kumar et al. [6], morphine-addicted animals were found to have decreased CD4+ T-cell count and increased set-point viral load compared to non-addicted animals. Many experimental studies have demonstrated the three major effects of drugs of abuse on the dynamics of HIV/SIV: (i) Drugs of abuse have been shown to increase expression of the CCR5 co-receptor in target cells, making them more susceptible to infection [5, 6, 25]; (ii) Opiates are known to diminish cellular immune responses [23, 24]; and (iii) the conditioning of the drugs of abuse is negatively correlated with SIV viral evolution and disease progression [21, 22, 23], indicating a lower mutation rate in the presence of drugs of abuse. While there is ample experimental evidence for these effects, their quantitative understanding is minimal. Therefore, the potential combined alteration in mutation, immune response, and cell susceptibility due to drugs of abuse need to be considered to quantify

the effects of opiate use on HIV infections.

Mathematical models have been previously used to study infectious diseases, including HIV/SIV [12, 19, 26, 27, 28, 29, 30, 31, 32, 33]. Models have also been developed to investigate viral escape [32, 33, 12], antibody responses [31], and viral evolution [19]. In this study, we present a mathematical model of HIV infection that incorporates morphine effects on the dynamics of viral replication, cellular immune responses, and mutation. We analyze the model to determine how morphine affects viral mutation and the long-term dynamics of mutant and wild-type virus species. We were able to fully characterize the dynamics using three steady-state solutions of the model: an infection-free steady state, a mutant-only steady state, and a coexistence steady state. Furthermore, we were able to show that the concentration of morphine present within the host is critical for the stability of the steady states of the virus-immune dynamical system.

2. Method

2.1. Mathematical model

2.1.1. Virus-cell dynamics

We extend the standard HIV dynamics model [26, 29] to include morphine effects on target cell susceptibility, viral mutation, and cellular immune response, which have been established in various experimental studies [5, 6, 21, 22, 23, 24, 25]. Following Vaidya et al. [30, 31], we include two populations of CD4+ target cells based on levels of CCR5 co-receptor expression: a population with lower susceptibility to infection, T_l, and a population with higher susceptibility to infection, T_h [5, 6, 25]. The viral mutation is modeled by including two viral species, a wild-type virus, V_w, and a mutant virus, V_m [13, 17]. We assume free virus particles infect target cells, resulting in corresponding infected cell populations, I_w and I_m. Cellular immune responses are represented by a population of CTLs, denoted by C, which directly kills infected cells [19, 34].

Target cells are recruited at a constant rate λ and are assumed to belong to the T_l population. Target cells switch from T_l to T_h at rate r and from T_h to T_l at rate q [30]. Both populations of target cells die at per capita rate δ_T [26, 29]. Target cells in the T_l population are infected by the wild-type virus at rate β_l and by the mutant virus at a rate $(1-F)\beta_l$, where F denotes the fitness cost of mutation, with $0 \leqslant F \leqslant 1$. Note that we assume the mutant virus to have a lower infection rate than the wild-type virus [33]. Similarly, T_h cells are infected at rates β_h and $(1-F)\beta_h$ by the

wild-type and mutant viruses, respectively. Due to mutation, a fraction ϵ of target cells infected by wild-type virus become mutant-infected cells, and the remaining $(1-\epsilon)$ stay wild-type infected cells [19].

Both virus species are produced by their corresponding infected cell population at rate p per cell and are cleared at rate δ_V [19]. We consider only forward mutation, i.e., target cells infected by the mutant virus do not revert to the wild-type infected population because the back mutation in the presence of morphine is not understood well. Wild-type infected cells, I_w, are killed by CTLs at rate b. Due to responses by epitope-specific CTLs, there is a reduced recognition of mutant-infected cells by the host's immune responses [19, 20]. We interpret this reduced rate as the escape rate. CTLs kill I_m cells at rate $\frac{b}{1+B}$, in which the base CTL killing rate b is reduced by the mutant escape ratio $1+B$. The mutant escape rate, $B>0$, represents a reduction in the ability of the host's cellular immune response to kill cells infected by the mutant virus compared to cells infected by the wild-type virus. Both classes of infected cells die at per capita rate δ_I. CTLs are produced at rate α per infected cell [19, 34], die at rate δ_C, and recruited at a constant rate ω [28], which also includes background production other than those proportional to infected cells.

2.1.2. Effects of morphine

Based on experimental results, we include the effects of morphine through three mechanisms: the higher transfer of T_l cells into T_h cells due to increased co-receptor expression [6, 25], the decrease in viral mutation [21, 22], and the decrease in CTL production [23]. We, therefore, make the transition parameters r and q morphine-dependent, i.e., $r=r(M)$ and $q=q(M)$, where M is the concentration of morphine. Since it is expected that $r(M)$ is an increasing function of morphine and $q(M)$ is a decreasing function of morphine, we model $r(M)$ and $q(M)$ using an E_{max} model as done previously [35],

$$\begin{aligned} r(M) &= r_c + (r_m - r_c)\eta_r(M), \\ q(M) &= q_m + (q_c - q_m)\eta_q(M), \end{aligned} \tag{1}$$

where

$$\begin{aligned} \eta_r(M) &= \frac{M^n}{M_h^n + M^n}, \\ \eta_q(M) &= 1 - \eta_r(M). \end{aligned} \tag{2}$$

Here, r_c and r_m are the minimum and maximum values of $r(M)$, q_c and q_m are the minimum and maximum values of $q(M)$, n is Hill's coefficient for the E_{max} model, and M_h is the morphine concentration that gives $r(M)$ and $q(M)$ the value half-way between their respective minimums and maximums. Since morphine causes a decrease in viral mutation [21, 22], we model the mutation rate as $\frac{\epsilon}{\mu+\eta M}$, where μ and η are parameters related to the effect of morphine on mutation. To model the decrease in CTL production due to morphine, we take the CTL recruitment rate as $\omega e^{-\psi M}$ and the CTL production rate in response to infection as $\frac{\alpha}{\gamma+\xi M}$, where ψ, γ, and ξ are parameters related to the decrease in CTL production due to morphine. The full model is given by the following seven-dimensional system of ODEs:

$$
\begin{aligned}
\frac{dT_l}{dt} &= \lambda + \left(q_m + (q_c - q_m)\left(1 - \frac{M^n}{M_h^n + M^n}\right)\right) T_h - \left(r_c + (r_m - r_c)\frac{M^n}{M_h^n + M^n}\right) T_l \\
&\quad - \beta_l V_w T_l - (1-F)\beta_l V_m T_l - \delta_T T_l, \\
\frac{dT_h}{dt} &= \left(r_c + (r_m - r_c)\frac{M^n}{M_h^n + M^n}\right) T_l - \left(q_m + (q_c - q_m)\left(1 - \frac{M^n}{M_h^n + M^n}\right)\right) T_h \\
&\quad - \beta_h V_w T_h - (1-F)\beta_h V_m T_h - \delta_T T_h, \\
\frac{dV_w}{dt} &= pI_w - \delta_V V_w, \\
\frac{dV_m}{dt} &= pI_m - \delta_V V_m, \\
\frac{dI_w}{dt} &= \left(1 - \frac{\epsilon}{\mu + \eta M}\right)(\beta_l V_w T_l + \beta_h V_w T_h) - bI_w C - \delta_I I_w, \\
\frac{dI_m}{dt} &= \frac{\epsilon}{\mu + \eta M}(\beta_l V_w T_l + \beta_h V_w T_h) + (1-F)(\beta_l V_m T_l + \beta_h V_m T_h) - \frac{b}{1+B} I_m C - \delta_I I_m, \\
\frac{dC}{dt} &= \omega e^{-\psi M} + \frac{\alpha}{\gamma + \xi M}(I_w + I_m) C - \delta_C C.
\end{aligned}
\tag{3}
$$

A schematic diagram of the model is shown in Figure 1.

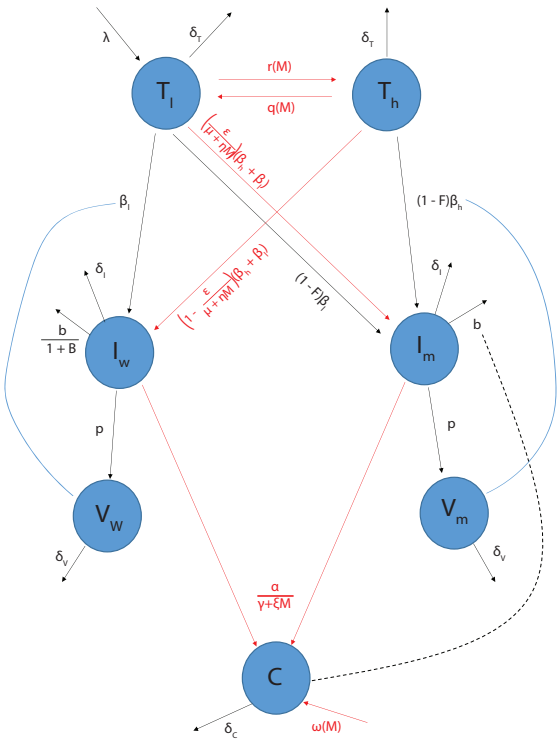

Figure 1: Schematic diagram of the model. The model includes two populations of target cells distinguished by susceptibility to infection, two viral strains and corresponding infected populations, and a cellular immune response in the form of CTLs. Viral species are distinguished by their infectivity rates and ability to escape from immune responses. Mechanisms that are affected by morphine, shown by red arrows, are the rate of viral mutation, target cell susceptibility, and production rate of CTLs.

2.2. Parameter estimation

We obtained some parameters from the literature and estimated some parameter values based on previously published studies. Following Vaidya et al. [30], we assume 10^6 target cells per ml of blood, with 40980 cells/ml belonging to the T_h population and the remaining 959020 cells/ml to the

T_l population. We assume that the infection begins with free virus only, and there are no infected cells, so we take $I_w(0), I_m(0) = 0$. Also, as described in Vaidya et al. [30], the SIV infection was established with 3×10^5 RNA copies of the virus. Assuming a macaque contains approximately 1.5 liters of extracellular water, we can estimate $V_0 = \frac{3 \times 10^5}{1.5L} \approx 200$ viral RNA copies/ml [30], which we assume to belong entirely to the V_w population. Estimates for $\lambda, \beta_l, \beta_h, r_c, r_m, q_m, q_c$, and δ_I were taken from Vaidya et al. [30], where these values were obtained by fitting the model to experimental data. In particular, they estimated β_h to be approximately two orders of magnitude higher than β_l. The viral production rate, p, is estimated from the SIV *in vivo* burst size in rhesus macaques and the average life span of an infected cell, giving $p = 2500$ per cell/day [30].

Based on modeling work by Stafford et al. [36], we take $\delta_T = 1/100 = 0.01$ per day, corresponding to a target cell life span of 100 days. Ramratnam et al. [37] give an estimated range of HIV viral clearance between 9.1 and 36 virions per day, so we use their average of 23 virions per day as our base value for δ_V. Mansky and Temin [38] determined the *in vivo* mutation rate of HIV-1 to be 3.4×10^{-5} mutations per base pair per generation, so we take the mutation rate $\epsilon = 3 \times 10^{-5}$. Following De Boer and Perelson [34], we take $\delta_C = 0.2$ per day as an estimate for the turnover of CTLs and $\alpha/\gamma = 6.7 \times 10^{-5}$ for the infected cell-dependent CTL production rate. Similar to other modeling works, we also include a constant production of CTLs $\omega = 15$ to include potential background production other than those proportional to infected cells [28, 39, 40].

Previous work by Ganusov et al. [33] investigated the rate of escape by mutant viruses from CTL responses. They measured the rate of escape by a single mutant variant as the average difference between the rate of mutant killing by CTLs and the production rate of the mutant. They consider the range of killing of infected cells (wild-type and mutant) by CTLs to be 0.01-0.5 per day, so we take $b = 0.25$ per day as our base value. In their study, the upper-value $b = 0.5$ corresponds to a wild-type virus, and the lower-value $b = 0.01$ to an escape mutant. Noting that $\frac{0.5}{0.01} = 50$, we will vary the escape ratio, B, from 0 to 50 with $B = 30$ as our base value [33].

In an experiment performed on children aged between two and six years, Olkkola et al. [41] observed initial morphine concentrations between 28 and 325 ug/l of blood plasma. To include this range, we will consider values of M to be between 0 and 200 ug/l [41]. Accordingly, we take $M_h = 100$, corresponding to the half-saturation value of $r(M)$ and $q(M)$. The estimated parameters and their descriptions are summarized in Table 1.

Table 1: Parameter Values

Parameter	Value (Range for LHS)	Description	Reference
λ	3690 (1500, 10000) ml/day	Production rate of T_l cells	[30]
$r(M)$	$r_c + (r_m - r_c)\eta_r(M)$ $(0.005, 2.7)$	Transition rate from T_l to T_h	[30]
$q(M)$	$q_c + (q_m - q_c)\eta_q(M)$ $(10^{-8}, 2.8)$	Transition rate from T_h to T_l	[30]
r_c	0.16 day^{-1}	Minimum value of r	[30]
r_m	0.52 day^{-1}	Maximum value of r	[30]
q_c	1.23×10^{-6} day^{-1}	Minimum value of q	[30]
q_m	0.25 day^{-1}	Maximum value of q	[30]
M_h	100 ug/l	Half morphine value for $r(M), q(M)$	[41]
n	8	Hill's coefficient of morphine response	[30]
β_l	10^{-9} $(10^{-11}, 10^{-5})$ ml/day	Wild- type infection rate of T_l cells	[30]
β_h	10^{-7} $(10^{-9}, 10^{-3})$ ml/day	Wild -type infection rate of T_h cells	[30]
F	0.1 $(0 - 1)$	Fitness cost of mutation	Assumed
p	2500 $(500, 5500)$ day^{-1}	Production rate of virus	[30]
b	0.25 $(0.005, 1.8)$ ml/day	CTL killing rate of wild-type	[33]
B	30 $(0.1, 100)$	Mutant escape ratio	Assumed
α	6.7×10^{-5} ml/day	CTL response to infection	[34]
γ	1	Morphine effect on α	Assumed
ξ	1 l/ug	Morphine effect on α	Assumed
ω	15 $(0.001, 40)$ ml/day	Base CTL production rate	Assumed
ψ	0.1 $(0.001, 1.5)$ ml/day	CTL prduction decay rate	Assumed
ϵ	3×10^{-5} $(3 \times 10^{-7}, 3 \times 10^{-3})$	Mutation rate	[38]
μ	1 $(0.01, 50)$	Morphine effect on ϵ	Assumed
η	1 $(0.01, 50)$ l/ug	Morphine effect on ϵ	Assumed
δ_T	0.01 $(0.001, 1.2)$ day^{-1}	Target cell death rate	[36]
δ_V	23 $(1, 50)$ day^{-1}	Virus clearance rate	[37]
δ_I	0.7 $(0.01, 10)$ day^{-1}	Infected cell death rate	[30]
δ_C	0.2 $(0.001, 1.6)$ day^{-1}	CTL death rate	[34]
M	$0 - 200$ ug/l	Concentration of morphine	[41]

3. Results

3.1. Basic reproduction number

The basic reproduction number, denoted by R_0, is defined as the average number of secondary infected cells resulting from a single initial infected cell when target cells are not limited [42]. R_0 is an important quantity in the study of viral dynamics that provides a threshold condition for infection to persist ($R_0 > 1$) and to die out ($R_0 < 1$).

We use the next-generation matrix method [43] to obtain an expression for the basic reproduction number of our model. The next-generation matrix is obtained from the infected subsystem of the model, i.e., the equations of the system corresponding to viruses and infected cells [43]. For our model, the infected subsystem is given by

$$\begin{aligned}
\frac{dV_w}{dt} &= pI_w - \delta_V V_w, \\
\frac{dV_m}{dt} &= pI_m - \delta_V V_m, \\
\frac{dI_w}{dt} &= (1-\hat{\epsilon}(M))(\beta_l V_w T_l + \beta_h V_w T_h) - bI_w C - \delta_I I_w, \\
\frac{dI_m}{dt} &= \hat{\epsilon}(M)(\beta_l V_w T_l + \beta_h V_w T_h) + (\hat{\beta}_l V_m T_l + \hat{\beta}_h V_m T_h) - \frac{b}{1+B} I_m C - \delta_I I_m,
\end{aligned} \tag{4}$$

where $\hat{\epsilon}(M) = \frac{\epsilon}{\mu+\eta M}$, $\hat{\beta}_l = (1-F)\beta_l$, and $\hat{\beta}_h = (1-F)\beta_h$. The infection-free equilibrium (IFE) is the steady-state solution of the model, in which all infected cell and virus populations are zero. For our model, we compute the IFE as $(T_l^*, T_h^*, 0, 0, 0, 0, C^*)$, where

$$\begin{aligned}
T_l^* &= \frac{\lambda(q(M)+\delta_T)}{\delta_T(q(M)+r(M)+\delta_T)}, \\
T_h^* &= \frac{\lambda r(M)}{\delta_T(q(M)+r(M)+\delta_T)}, \\
C^* &= \frac{\hat{\omega}(M)}{\delta_C},
\end{aligned} \tag{5}$$

and $\hat{\omega}(M) = \omega e^{-\psi M}$. Now, we linearize the infected subsystem about the IFE and decompose it into $\mathcal{F} - \mathcal{V}$, where $\mathcal{F}$ is the part of the system that describes newly infected components, and $\mathcal{V}$ is the part that describes transitions of cells and viruses in and out of compartments. $\mathcal{F}$ and $\mathcal{V}$ for

our model are given by

$$\mathcal{F} = \begin{bmatrix} 0 & 0 & 0 & 0 \\ 0 & 0 & 0 & 0 \\ (1-\hat{\epsilon}(M))(\beta_l T_l^* + \beta_h T_h^*) & 0 & 0 & 0 \\ \hat{\epsilon}(M)(\beta_l T_l^* + \beta_h T_h^*) & (\hat{\beta}_l T_l^* + \hat{\beta}_h T_h^*) & 0 & 0 \end{bmatrix} \tag{6}$$

and

$$\mathcal{V} = \begin{bmatrix} \delta_V & 0 & -p & 0 \\ 0 & \delta_V & 0 & -p \\ 0 & 0 & \delta_I + bC^* & 0 \\ 0 & 0 & 0 & \delta_I + \frac{b}{1+B}C^* \end{bmatrix}. \tag{7}$$

The next-generation matrix is $\mathcal{F}\mathcal{V}^{-1}$ [43]. The basic reproduction number of our model is then obtained as the spectral radius of $\mathcal{F}\mathcal{V}^{-1}$, i.e., $R_0 = \sigma(\mathcal{F}\mathcal{V}^{-1}) = \max\{R_0^w, R_0^m\}$, where

$$\begin{aligned} R_0^w &= \frac{(1-\hat{\epsilon}(M))(\beta_h T_h^* + \beta_l T_l^*)p}{\delta_V(bC^* + \delta_I)} \quad \text{and} \\ R_0^m &= \frac{(1-F)(\beta_h T_h^* + \beta_l T_l^*)(1+B)p}{\delta_V(\delta_I B + bC^* + \delta_I)} \end{aligned} \tag{8}$$

represent the basic reproduction number corresponding to the wild-type and mutant virus, respectively. Note that since $\hat{\epsilon}(M), T_l^*, T_h^*$, and C^* are morphine dependent, R_0^w and R_0^m are also morphine dependent. In addition, if $R_0^w < 1$ and $R_0^m < 1$ the infection will die out while if either $R_0^w > 1$ or $R_0^m > 1$ the infection will be established [42]. Using the parameter values in Table 1, we compute $R_0^w = 0.08$, $R_0^m = 1.07$, and $R_0 = max\{R_0^w, R_0^m\} = 1.07 > 1$, indicating that the infection persists for this basic parameter set.

To study the effect of each parameter on R_0, we first determine the local sensitivity of R_0^w and R_0^m to changes in individual parameters. For a parameter ρ of the model, the forward sensitivity index is given by

$$S_\rho = \frac{\rho}{R_0}\frac{\partial R_0}{\partial \rho}. \tag{9}$$

Then S_ρ determines the relative instantaneous change in R_0 caused by a change in ρ [44, 45, 46]. The higher the values of S_ρ, the more sensitive R_0 is to ρ. Also, positive (negative) values of S_ρ

indicate that R_0 increases (decreases) as ρ increases. Sensitivity indices for R_0^w and R_0^m are shown in Figure 2 (left). We found that R_0^w and R_0^m are positively correlated to λ, r, p, and δ_C, indicating that an increase in these parameters is favorable for an infection to occur. This is expected since increasing λ, r, and δ_C will result in more (susceptible) target cells available for infection while increasing p results in more virions that can infect target cells. On the other hand, R_0^w and R_0^m are negatively correlated to q, b, δ_T, δ_V, and ω. Increased δ_T and δ_V cause increased death of target cells and viral clearance, respectively, both unfavorable for the virus, while a larger ω means more CTLs are responding to the infection. Larger values of parameter q increase target cells in the lower susceptibility population, and increased CTL killing rate b indicates a stronger immune response. Both of these mechanisms are also unfavorable to the virus. In addition, R_0^m is positively related to B and negatively related to F since a mutant virus benefits from a higher rate of immune escape and lower fitness of mutation. We found that R_0^w and R_0^m are less sensitive to changes in β_l, β_h, ϵ, μ, η or ψ on these base-case parameters.

To further quantify the global sensitivity of R_0^w and R_0^m to the parameters, we used Latin hypercube sampling (LHS) to obtain 10,000 samples of parameter sets. We used these parameters to calculate corresponding R_0^w and R_0^m values. In LHS, individual parameter values were sampled uniformly from the interval $[\rho_{min}, \rho_{max}]$ for each parameter ρ, where ρ_{min} and ρ_{max} were selected to give a realistic range of values (Table 1). The PRCCs of rank-transformed data were then calculated as the Pearson correlation coefficient between the vectors of selected values and the reproductive numbers [44].

The obtained partial rank correlation coefficients are shown in Figure 2 (right). The LHS-based sensitivities are consistent with the forward sensitivity indices, but the magnitude of sensitivity is relatively lower in general. Here also, λ, r, p, and δ_C, i.e., those related to increased amounts of virus and susceptible target cells, are mostly associated with more infectious viruses. Similarly, higher values of the CTL killing rate b, death rates $\delta_T, \delta_V, \delta_I$, and CTL production rate ω lead to more viruses. Note that R_0^w is unaffected by changes in F and B since these parameters only relate to the viability of the mutant virus. The mutant benefits from a low fitness cost and high rate of immune escape, which is reflected in R_0^m being positively associated with B and negatively associated with F.

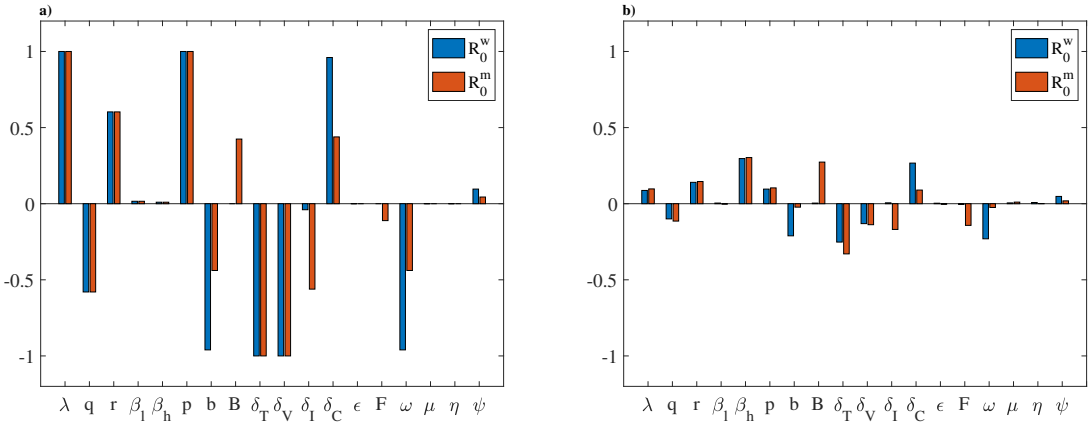

Figure 2: Local sensitivity indices (left) and partial rank correlation coefficients from 10,000 LHS for R_0^w and R_0^m. A positive value is favorable to the virus infection while a negative value is unfavorable to the viral infection. The higher the magnitude of the sensitivity value, the more sensitive R_0 is to the parameter.

3.2. Virus species switch

The viral species with a larger reproduction number can be considered to be the dominant species. For the base case with $M = 0$ we obtained $R_0^w = 0.08$ and $R_0^m = 1.07$, indicating that the mutant is the dominant viral population. An increase in M increases both R_0^w and R_0^m, and so R_0. For example, $M = 200$ causes R_0^w, R_0^m, and R_0 to become 5.6, 5.05, and 5.6, respectively. We found that increasing the amount of morphine past a threshold value, M_{thresh}, results in a viral species switch. The wild-type becomes the dominant viral population when the morphine concentration exceeds M_{thresh} (Figure 3).

The value of M_{thresh} can be determined by solving $R_0^w(M) = R_0^m(M)$ for M. For $M < M_{thresh}$, the mutant dominates, and for $M > M_{thresh}$, the wild-type dominates. Due to the nonlinearity in R_0^w and R_0^m, we did not find a closed form for M_{thresh} and obtained it numerically. For our base parameter values, $M_{thresh} \approx 54$, the wild-type is the dominant population for $M > 54$, and the mutant dominates for $M < 54$.

We now evaluate the effect of F (fitness cost) and B (immune escape) on M_{thresh}. As predicted by our model (Figure 3), in general, M_{thresh} decreases as F increases and/or B decreases. For a substantially higher fitness cost (for example, $F > 0.93$ in our computations), the mutant population is not fit enough to out-compete the wild-type, and the wild-type always dominates for any values

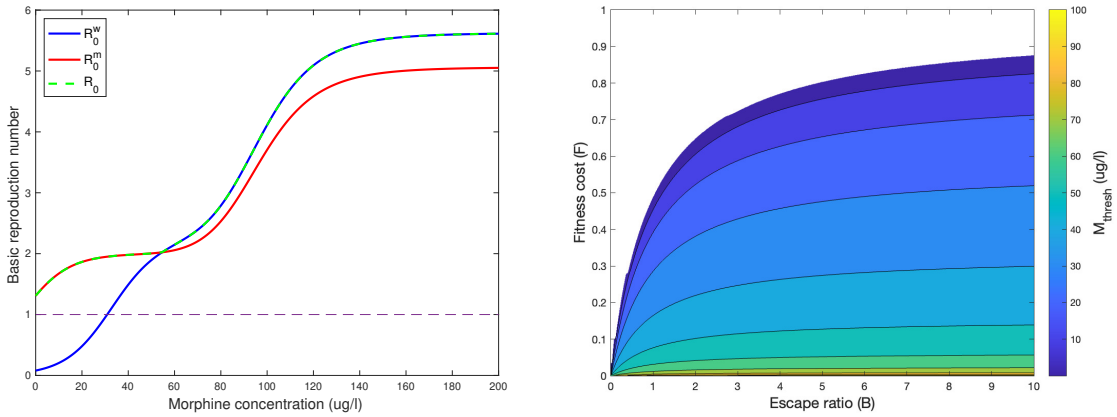

Figure 3: (Left) R_0^w and R_0^m as functions of M. With parameter values as in Table 1, $M_{thresh} \approx 54$ ug/ml. The mutant is the dominant population for $M < 54$ ug/ml and the wild-type is dominant for $M > 54$ ug/ml. (Right) M_{thresh} in $F - B$ parameter space. An increase in fitness cost (F) or a decrease in escape ratio B causes an increase in M_{thresh} value. The upper-left region represents (F, B) values that cause the wild-type to always dominate.

of M. On the other hand, for a low enough B ($B < 0.12$ in our computations), we did not find any value of M_{thresh} because CTLs are highly effective against the mutant virus, and the mutant virus cannot out-compete the wild-type virus.

3.3. Stability of steady-states

3.3.1. Infection-free equilibrium

The IFE is shown in Section 3.1. As discussed earlier, the local stability of the IFE is determined by the basic reproduction number. It is easy to prove that the IFE is locally asymptotically stable if $R_0 < 1$ and unstable if $R_0 > 1$ [42].

3.3.2. Wild-type only equilibrium

A wild-type only equilibrium is a solution, $(T_l^*, T_h^*, V_w^*, 0, I_w^*, 0, C^*)$, of the following system of equations

$$\begin{aligned}
0 &= \lambda + q(M)T_h^* - r(M)T_l^* - \beta_l V_w^* T_l - \delta_T T_l^*, \\
0 &= r(M)T_l^* - q(M)T_h^* - \beta_h V_w^* T_h^* - \delta_T T_h^*, \\
0 &= pI_w^* - \delta_V V_w^*, \\
0 &= (1-\hat{\epsilon}(M))(\beta_l V_w^* T_l + \beta_h V_w^* T_h^*) - bI_w^* C^* - \delta_I I_w^*, \\
0 &= \hat{\epsilon}(M)(\beta_l V_w^* T_l^* + \beta_h V_w^* T_h^*), \\
0 &= \hat{\omega}(M) + \hat{\alpha}(M) I_w^* C - \delta_C C^*.
\end{aligned} \tag{10}$$

Solving the second equation for T_h^* gives:

$$T_h^* = \frac{r(M)}{q(M) + \beta_h V_w^* + \delta_T} T_l^*, \tag{11}$$

and, since $\hat{\epsilon}(M) \neq 0$, the fifth equation is equivalent to

$$0 = \beta_l V_w^* T_l^* + \beta_h V_w^* T_h^*. \tag{12}$$

This implies $V_w^* = 0$, which corresponds to the IFE, or

$$0 = T_l^* \Big(\beta_l + \beta_h \Big(\frac{r(M)}{q(M) + \beta_h V_w^* + \delta_T} \Big) \Big). \tag{13}$$

Then either $T_l^* = 0$ or $\beta_l + \beta_h(\frac{r(M)}{q+\beta_h V_w^* + \delta_T}) = 0$. Substituting $T_l^* = 0$ into the first equation gives the negative solution $T_h^* = -\frac{\lambda}{q(M)}$. Also, letting $\beta_l + \beta_h(\frac{r(M)}{q(M)+\beta_h V_w^* + \delta_T}) = 0$, we get

$$V_w^* = -\frac{1}{\beta_h} \Big(\frac{\beta_h r(M)}{\beta_l} + q(M) + \delta_T \Big), \tag{14}$$

which is also a negative solution. Therefore, the system does not provide a wild-type only equilibrium. This is expected because the wild-type virus promotes a fraction of infections transitioned to the mutant population due to mutation.

3.3.3. Mutant-only equilibrium

The mutant only equilibrium (MOE) is the steady-state solution of the model, in which only the mutant population exists. The MOE of our model takes the form $(\hat{T_l}, \hat{T_h}, 0, \hat{V_m}, 0, \hat{I_m}, \hat{C})$, where

$$\begin{aligned}
\hat{T_h} &= \frac{r(M)\lambda}{(q(M)+\hat{\beta}_h\hat{V}_m+\delta_T)(r(M)+\hat{\beta}_l\hat{V}_m+\delta_T)-r(M)q(M)},\\
\hat{T_l} &= \frac{\lambda(q(M)+\hat{\beta}_h\hat{V}_m+\delta_T)}{(q(M)+\hat{\beta}_h\hat{V}_m+\delta_T)(r(M)+\hat{\beta}_l\hat{V}_m\delta_T)-r(M)q(M)},\\
\hat{I_m} &= \frac{\delta_V\hat{V}_m}{p},\\
\hat{C} &= \frac{\hat{\omega}(M)}{\delta_C-\hat{\alpha}\frac{\delta_V\hat{V}_m}{p}},
\end{aligned} \tag{15}$$

and $\hat{V}_m$ is the solution of

$$g(\hat{V}_m) = 0, \tag{16}$$

with

$$\begin{aligned}
g(\hat{V}_m) = &\frac{\hat{\beta}_l\hat{V}_m\lambda\left(\hat{V}_m\hat{\beta}_h+q(M)+\delta_T\right)+\hat{\beta}_h r(M)\hat{V}_m\lambda}{\left(\hat{V}_m\hat{\beta}_h+q(M)+\delta_T\right)\left(\hat{V}_m\hat{\beta}_l+r(M)+\delta_T\right)-r(M)q(M)}\\
&-\frac{b\delta_V\hat{V}_m\hat{\omega}}{(1+B)\,p\left(\delta_C-\frac{\hat{\alpha}\delta_V V_m^*}{p}\right)}-\frac{\delta_I\delta_V\hat{V}_m}{p}.
\end{aligned}$$

Clearly, $\hat{V}_m = 0$ is a solution that corresponds to the IFE. We now obtain solutions with $\hat{V}_m > 0$. We can obtain a value for $\hat{V_m}$ by solving (1) numerically, and substituting into the expressions for $\hat{T_h}, \hat{T_l}, \hat{I_m}$, and $\hat{C}$. Geometrically, $\hat{V_m}$ can be represented by the intersection of the curve $g(\hat{V}_m)$ and the axis $g = 0$. As shown in Figure 4a, the steady-state value of $\hat{V}_m$ at the MOE is the x-intercept of the curve $g(\hat{V}_m)$. We observe that the higher morphine concentrations intersect the x-axis further to the right. These $\hat{V}_m$ values at MOE can be substituted into the expressions for the other variables at MOE. A graph of $\hat{V}_m$ as a function of M (Figure 4b) shows that increasing M causes a larger non-zero equilibrium value of $\hat{V_m}$, indicating a higher set point viral load for larger morphine concentrations, consistent with experimental data [6]. Moreover, increasing M reduces values of T_l, T_h, and C, and increases the value of I_m at the MOE (Figure 4c-f)). Combining all

these results, we conclude that morphine causes infection of more target cells and less killing of infected cells by CTLs at the MOE.

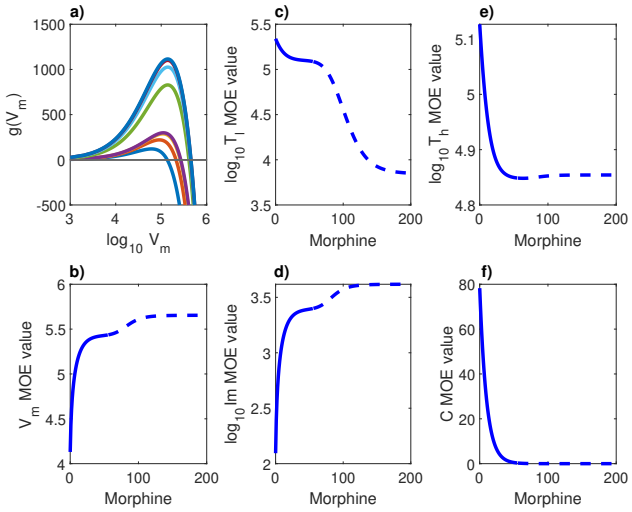

Figure 4: (a) Graphs of $g(V_m)$ (Eq. 16) for different morphine levels. Each color represents a different value of M, and the x-intercept of each curve represents the steady-state viral load at the MOE. (b - f) V_m, T_l, T_h, I_m, and C steady-state values at MOE. Morphine is varied along the x-axis, and the y-axis represents the steady-state value at the MOE. The solid portion of each curve represents locally-stable equilibria, and the dashed portions represent unstable equilibria.

To determine the local stability of the MOE, we calculate the eigenvalues of the Jacobian matrix, J, of the model evaluated at the MOE, given by

$$J = \begin{bmatrix} J_{11} & J_{12} & J_{13} & J_{14} & 0 & 0 & 0 \\ J_{21} & J_{22} & J_{23} & J_{24} & 0 & 0 & 0 \\ 0 & 0 & J_{33} & 0 & J_{35} & 0 & 0 \\ 0 & 0 & 0 & J_{44} & 0 & J_{46} & 0 \\ J_{51} & J_{52} & J_{53} & 0 & J_{55} & 0 & J_{57} \\ J_{61} & J_{62} & J_{63} & J_{64} & 0 & J_{66} & J_{67} \\ 0 & 0 & 0 & 0 & J_{75} & J_{76} & J_{77} \end{bmatrix}, \tag{17}$$

where

$$
\begin{aligned}
J_{11} &= -r(M) - \beta_l V_w - \hat{\beta}_l V_m - \delta_T, & J_{52} &= (1-\hat{\epsilon}(M))\beta_h V_w,\\
J_{12} &= q(M), & J_{53} &= (1-\hat{\epsilon}(M))(\beta_l T_l + \beta_h T_h),\\
J_{13} &= -\beta_l T_l, & J_{55} &= -bC - \delta_I,\\
J_{14} &= -\hat{\beta}_l T_l, & J_{57} &= -bI_w,\\
J_{21} &= r(M), & J_{61} &= \hat{\epsilon}(M)(\beta_l V_w + \hat{\beta}_l V_m),\\
J_{22} &= -q(M) - \beta_h V_w - \hat{\beta}_h V_m - \delta_T, & J_{62} &= \hat{\epsilon}(M)\beta_h V_w + \hat{\beta}_h V_m,\\
J_{23} &= -\beta_h T_h, & J_{63} &= \hat{\epsilon}(M)(\beta_l T_l + \beta_h T_h),\\
J_{24} &= -\hat{\beta}_h T_h, & J_{64} &= \hat{\beta}_l T_l + \hat{\beta}_h T_h,\\
J_{33} &= -\delta_V, & J_{66} &= -\tfrac{b}{1+B}C - \delta_I,\\
J_{35} &= p, & J_{67} &= -\tfrac{b}{1+B}I_m,\\
J_{44} &= -\delta_V, & J_{75} &= \hat{\alpha}(M)C,\\
J_{46} &= p, & J_{76} &= \hat{\alpha}(M)C,\\
J_{51} &= (1-\hat{\epsilon})\beta_l V_w, & J_{77} &= \hat{\alpha}(M)(I_w + I_m) - \delta_C.
\end{aligned}
$$

The MOE is locally asymptotically stable if the real part of each eigenvalue of J is negative and unstable otherwise [47, 48]. We determined the stability of the MOE by computing the eigenvalues of $J(MOE)$ for $M \in [0, 200]$. We observed that each eigenvalue of $J(MOE)$ had a negative real part for $M < M_{thresh}$ and that the real part of one eigenvalue became positive for $M > M_{thresh}$, indicating that the MOE becomes unstable for larger morphine concentrations. This is consistent with the viral species switch presented in Section 3.2, in which the larger values of M allow the wild-type virus to dominate.

3.3.4. Coexistence equilibrium

Due to the model's non-linear nature, we could not obtain an analytical expression for the coexistence equilibrium. However, by examining eigenvalues numerically, we determined that the coexistence equilibrium is locally asymptotically stable when $M > M_{thresh}$. A high morphine concentration (larger than M_{thresh}) allows the wild-type virus to dominate, in which case a small amount of mutant persists due to mutation, resulting in a coexistence equilibrium.

3.3.5. Parameter space and stability for equilibrium

In this section, we numerically investigate the effects of F (mutant fitness cost) and B (immune escape rate) on the stability of the model equilibria by examining R_0^w and R_0^m under the conditioning

of various morphine (M) levels. The stability regions in the $M-F$ and $M-B$ planes are presented in Figure 5. Depending on the combination of M, F, and B, the model evolves to one of the three biologically relevant equilibria based on local stability analysis: (a) If $R_0^w < 1$ and $R_0^m < 1$, the model converges to the IFE; (b) If $R_0^w < 1$ and $R_0^m > 1$, the model converges to the MOE; and (c) If $R_0^w > 1$ and $R_0^w > R_0^m$, the model converges to the coexistence equilibrium (CE).

In Figure 5(left) we present the region in the $M-F$ plane, at which each equilibrium is stable. It is interesting to note that the IFE-MOE and MOE-CE boundaries are quite nonlinear. We observe that a lower fitness cost and lower morphine concentration can cause the MOE to be stable. Similarly, a higher fitness cost and lower morphine concentration result in the stability of infection-free equilibrium. For a substantially higher morphine concentration, the coexistence equilibrium becomes stable regardless of fitness cost, promoting both virus species to survive in the system.

In Figure 5(right), we present the region in the $M-B$ plane for the stability of each equilibrium. In this case, the boundary between the IFE-MOE and MOE-CE is nonlinear, and there is no boundary separating the IFE and CE. As predicted by our model, a smaller B and a lower morphine concentration allow the IFE to become stable. However, a higher B causes the MOE to be stable at a lower level of morphine concentration. Regardless of the escape ratio B, sufficiently high morphine concentration implies the stability of coexistence equilibrium, and both viruses survive in the system.

In summary, a high morphine concentration favors the wild-type virus regardless of other parameter values. Since some mutant virus is always produced from the wild-type, this makes CE the stable equilibrium. The MOE is stabilized by low morphine, a low fitness cost, and high chance of immune escape. At a sufficiently lower morphine concentration, high fitness cost and low escape ratio result in a stable IFE, thereby controlling the infection.

3.4. Effects of morphine on virus-cell dynamics: Model simulations

We now present the model simulations to observe the effects of morphine on the virus-cell dynamics. Since $R_0 > 1$ for our base parameter values, we expect that the infection is established for any concentrations of morphine, as revealed in the simulations (Figure 6a). We found $\sim$1.5 $\log_{10}$ increase in set-point viral load (Figure 6a) and $\sim$300 count decrease in CD4 (Figure 6b) for the morphine conditioning of $M = 200$ compared to the absence of morphine ($M = 0$), consistent

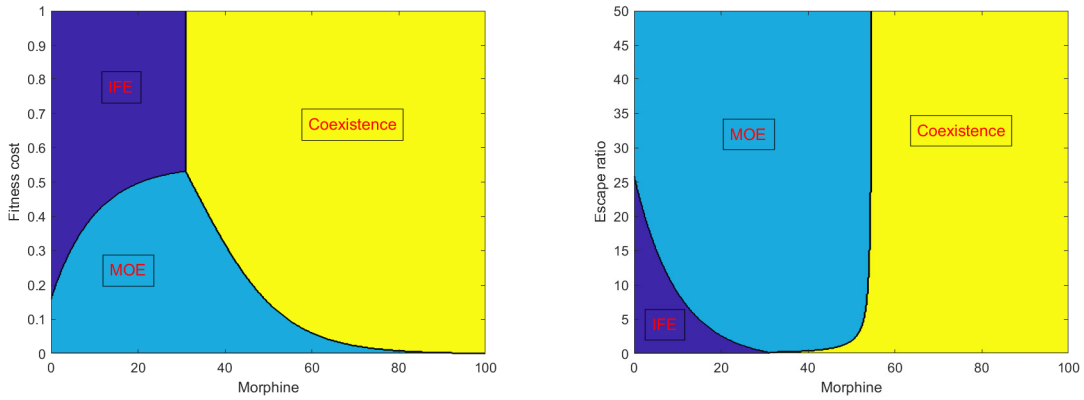

Figure 5: Model predicted stability regions for Infection-Free Equilibirum (dark-blue), Mutant-Only Equilibrium (light-blue) and Coexistence Equilibirum (yellow) in $M - F$ space (left, with $B = 30$) and $M - B$ space (right, with $F = 0.1$).

with the experimental results [6].

We also present the dynamics of wild-type and mutant virus in the absence ($M = 0$, Figure 6c) and presence ($M = 200$, Figure 6d) of morphine. For $M = 0$, the mutant virus quickly out-competes with the wild-type, and in the long run, the viral load consists entirely of the mutant population, with the wild-type population going extinct (Figure 6c). If excessive morphine is in the system, i.e., $M = 200$, both virus species co-exist, with the wild-type population dominating the mutant population (Figure 6d).

To investigate the altered viral dynamics due to the presence of morphine on the effectiveness of antiretroviral therapy (ART), we introduced ART via reverse transcriptase and protease inhibition [49]. These drugs can be introduced into our model by performing the following transformations: $\beta_i \to (1 - \Phi)\beta_i, i = l, h$ (reverse transcriptase inhibitors), and $p \to (1 - \Psi)p$ (protease inhibitors), where Φ and Ψ are efficacy of corresponding ARTs. In Figure 7, we present simulations of a course of ARTs with 90% efficacy initiated at the steady state. In Figure 7 (left), we present the viral dynamics in the absence and presence of morphine both before and after ART treatment. We observed that the combined morphine effects in our model caused 7 days longer for the viral load to reach the detection limit (50 viral RNA copies per ml) (Figure 7 left). In Figure 7 (right), we first simulate the viral dynamics until a steady state with M = 200 (presence of morphine). Once a steady state is reached, we began ART under two conditions: one without morphine (M=0) and

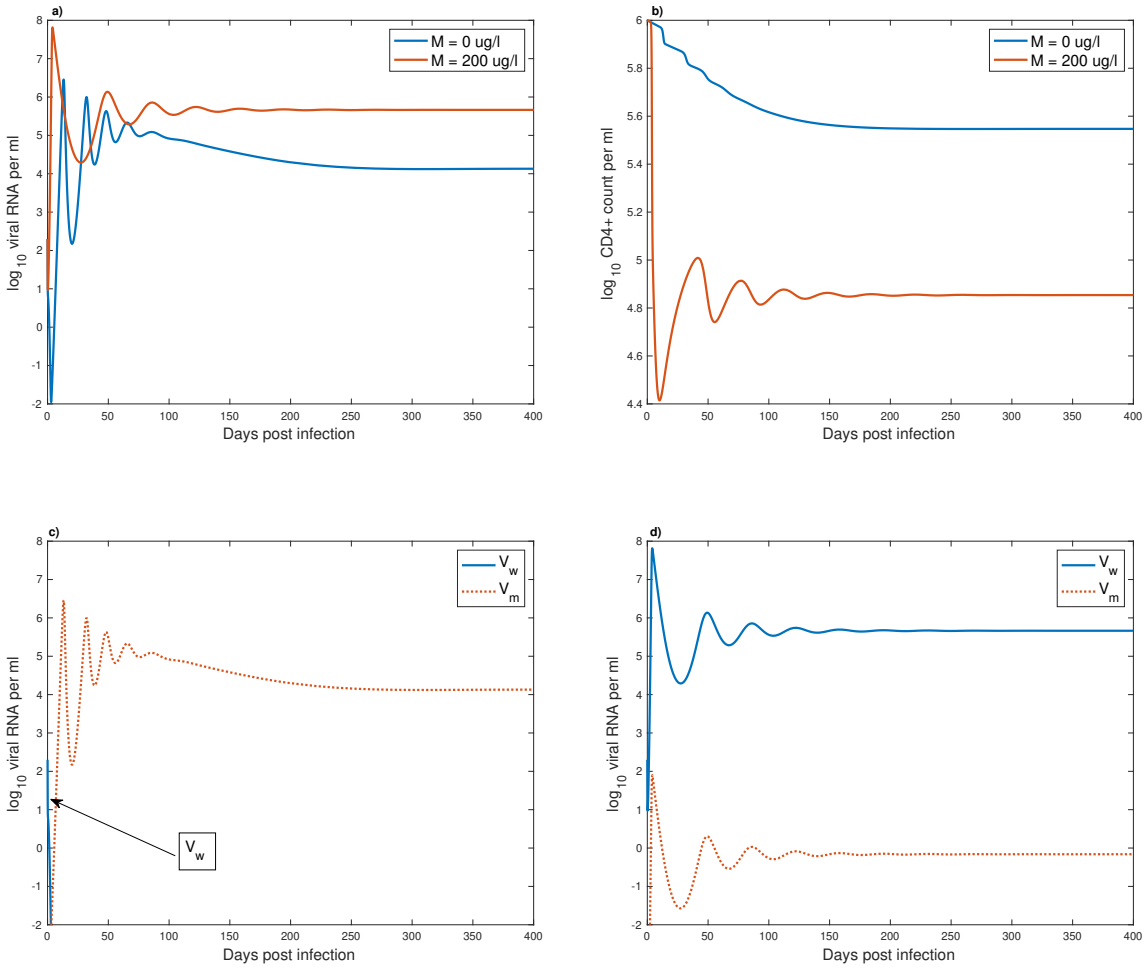

Figure 6: (a) Model predicted viral load and (b) CD4+ count for 400 days post-infection for absence ($M = 0$) and presence ($M = 200$) of morphine. Dynamics of the wild-type and mutant virus populations in (c) the absence ($M = 0$) and (d) the presence ($M = 200$) of morphine.

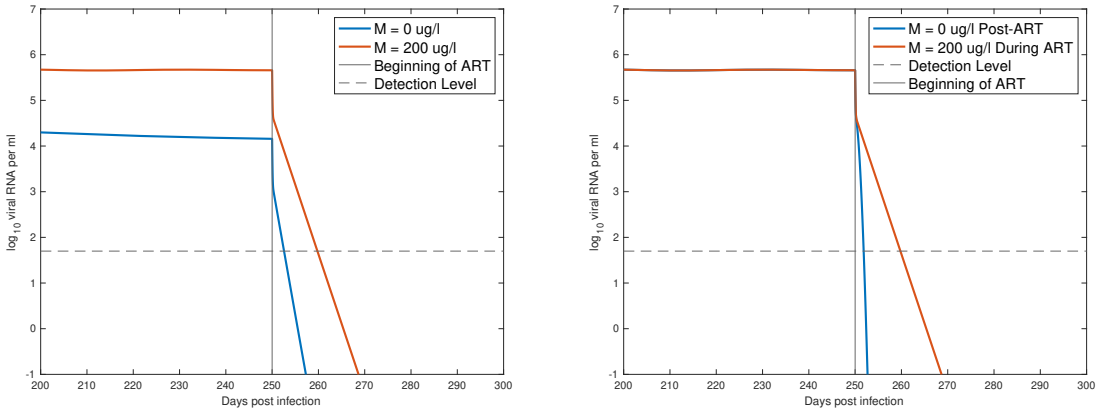

Figure 7: Model simulation of a course of antiretroviral therapy. (Left) ART was started after the model was allowed to come to steady state. When morphine is not being used (blue), the model predicts a 2 day lag for the virus to become undetectable versus 9 days when morphine is being used (red). (Right) After reaching the steady state under morphine conditioning, ART was initiated with two conditions: one in the absence of post-ART morphine (blue) and another in the presence of post-ART morphine (red).

another with M = 200. These two conditions represent the first patient who stops taking drugs of abuse once ART begins and the second patient who continues taking drugs of abuse even after ART. This result (Figure 7 (right)) further confirms that the viral load falls below the detection limit faster when morphine is not present.

3.5. Sensitivity of viral load and CD4+ count

Here we investigate the sensitivity of set-point viral load and CD4+ count to parameter changes under various morphine concentrations. For each parameter ρ, 10,000 values were sampled via LHS from an interval $[\rho_{min}, \rho_{max}]$ with lower- and upper-bounds chosen to give a wide range of biologically-relevant values (Table 1). After sampling, PRCCs were computed as the Pearson correlation coefficient between the model output and sampled parameter values [44].

Figure 8 (a) and (b) show the PRCCs between the parameters and set-point viral loads for $M = 0$ and $M = 200$, respectively. Similarly, Figure 8 (c) and (d) show the PRCCs between parameters and CD4+ counts for $M = 0$ and $M = 200$, respectively. Total viral load and CD4+ are both positively associated with target cell recruitment λ. Viral load is positively associated with virus production p and negatively associated with the death parameters δ_T and δ_V. CD4+

counts are most negatively associated with the transition rate r and positively associated with viral clearance δ_V.

In the absence of morphine (Figure 8a), the total viral load is more sensitive to the fitness cost F because the mutant virus is dominant, and a higher fitness cost corresponds to a weaker virus. When morphine is in use (Figure 8b), the infected cell death rate δ_I had a higher global sensitivity as well. Similarly, in the absence of morphine (Figure 8c), CD4+ counts were more sensitive to F as well as to CTL-related parameters b, ω, and δ_C compared to the high morphine case (Figure 8d). This is expected since the lower morphine case has a stronger response by CTLs and those parameters have a larger effect.

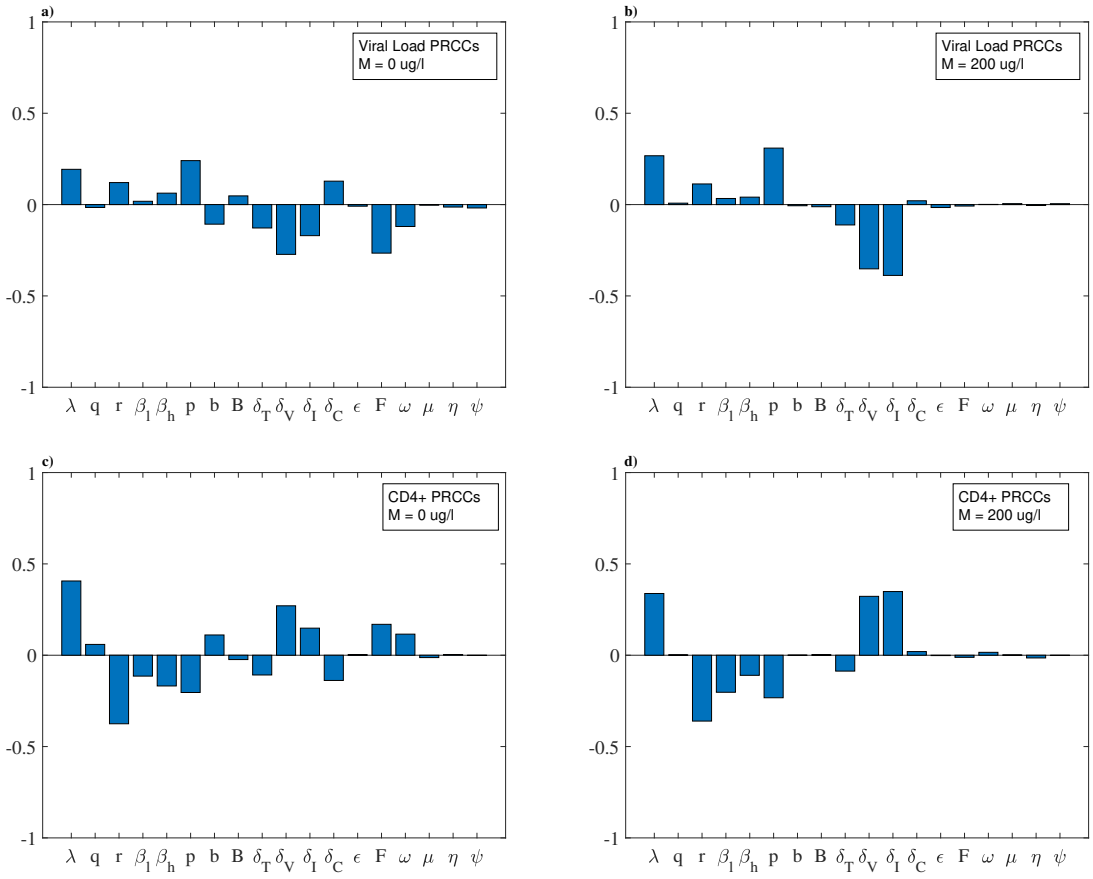

Figure 8: The partial rank correlation coefficients obtained from Latin hypercube sampling method for set-point viral load (a,b) and CD4+ count (c,d) in the absence ($M = 0$) and in the presence ($M = 200$) of morphine.

4. Conclusion

HIV is an ongoing public health problem worldwide, and the recreational use of injection drugs is one of the main risk factors for contracting it [2]. In addition to increasing the risk of contracting HIV, injection drug use has been shown to have several adverse effects, such as a faster progression to AIDS, a higher chance of HIV-related neurological complications, increased set-point viral load, and decreased immune response [6, 7]. In this study, we developed a mathematical model of HIV dynamics to investigate the effect of drugs of abuse (morphine) on viral load, immune responses, and viral mutation. This model expands on previous models of HIV wild-type-mutant dynamics with the inclusion of morphine-affected mechanisms [19, 50]. We analyzed our model to determine the short- and long-term outcome of an HIV infection in the presence of drugs of abuse.

We identified three biologically-relevant equilibria of our model and characterized their stability in terms of the morphine level present in the system, the fitness cost of mutation of the virus, and the viral escape ratio. Using numerical techniques, we were able to identify the threshold morphine concentration that determines whether the wild-type or mutant virus dominates, M_{thresh}. We also found $\sim$1.5 $\log_{10}$ increase in set-point viral load and $\sim$300 count decrease in CD4 when morphine was present in the body of an infected host.

Since morphine inhibits CTL responses, our model predicted a higher set-point viral load in the presence of morphine. Notably, our model showed that wild-type virus dominates in morphine conditioning due to a diminished viral mutation caused by morphine. We also found that a low fitness cost and high escape ratio lead to a state where the wild-type virus goes extinct as the mutant virus out-competes, and the virus population is entirely mutant (the mutant-only equilibrium). On the other hand, high morphine gives an advantage to the wild-type virus, increasing the total viral load with the wild-type virus dominating.

Several clinically relevant insights can be gleaned from our model. Our model prediction related to competition dynamics of two viral species influenced by drug use has not been studied experimentally; the results in this paper may motivate such clinical work. A longer time for viral suppression due to ART treatment for morphine conditioning provides important implications for designing treatment protocols for drug-addicted individuals. Other modeling studies with wild-type and mutant viruses have investigated treatment strategies when the mutant is resistant to ART [50]. One of the bases of our model presented here is the decrease in viral mutation due to morphine [21, 22]. Our modeling results can also be relevant to the potential reduction of the emergence

of ART resistance in the drug-addicted group, thereby providing useful information for successful treatment strategies for drug abusers.

Our model has several limitations. The body metabolizes morphine, and its concentration decreases over time [41]. We assumed a constant morphine concentration, M, and used this value in the analysis of the model. Future work should include time-dependent concentrations using the pharmacokinetics of morphine. Additionally, long-term infection dynamics may be impacted by antibody responses and the presence of latently infected cells [28, 31]. Including these factors in the model may improve our understanding of viral dynamics and mutation under morphine conditioning. Based on previous studies on HIV, we only considered the fitness cost of mutation. If there is a chance that mutation can result in a more fit mutant with an additional advantage over the wild-type, future investigations may need to consider viral mutation with virus species of various fitnesses. Our model assumed the increased viral load under morphine conditioning is only related to morphine use, as adopted in the experiments. However, we acknowledge that more severe diseases could also be due to other factors related to drug use, such as poor diet or lifestyle. Also, further experimental data with frequent measurement of viral loads, virus species populations, and CTLs may help strengthen those effects of morphine introduced into the model.

To summarize, we developed a novel model to investigate the effects of morphine on within-host dynamics of wild-type and mutant HIV species. Our model predicts that the role of morphine in increased susceptibility of the target cells, decreased CTL responses, and decreased mutation eventually results in an increase in set-point viral load and a decrease in CD4 count. We identified three biologically relevant steady-states of our model and characterized them based on morphine concentration, the fitness cost of mutation, and viral escape. Our results may help design proper control measures for HIV infection within drug abusers.

Acknowledgement

This work was funded by NSF grants DMS-1951793, DMS-1836647, and DMS-1616299 from National Science Foundation, the United States, and the UGP award and the start-up fund (NKV) from San Diego State University. The funders had no role in study design, data collection, analysis, decision to publish, or manuscript preparation.

References

[1] UNAIDS. UNAIDS Data 2021 (2021).

[2] Alcabes, P.; Friedland, G. Injection drug use and human Immunodeficiency Virus Infection. *Clin. Infect. Dis.* **1995**, 20, 1467–1479.

[3] Fauci, A. S. Pathogensis of HIV disease: Opportunities for new prevention interventions. *Clin. Infect. Dis.* **2007**, 45, S206-S212.

[4] Kohli, R.; Lo, Y.; Howard, A. A.; Buono, D.; Floris-Moore, M.; Klein, R. S.; Schoenbaum, E. E. Mortality in an Urban Cohort of HIV-Infected and At-Risk Drug Users in the Era of Highly Active Antiretroviral Therapy. *Clin. Infect. Dis.* **2005**, 41, 864-872.

[5] Li, Y.; Wang, X.; Tian, S.; Guo, C.; Douglas, S. D.; Ho, W. Methadone enhances human immunodeficiency virus infection of human immune cells. *J. Infect. Dis.* **2002**, 185, 118-122.

[6] Kumar, R.; Torres, C.; Yamamura, Y.; Rodriguez, I.; Martinez, M.; Staprans, S.; Donahoe, R. M.; Kraiselburd, E.; Stephens, E. B.; Kumar, A. Modulation by morphine of viral set point in rhesus macaques infected with simian immunodeficiency virus and simian-human immunodeficiency virus. *J. Virol.* **2004**, 78, 11425-11428.

[7] Hauser, K. F.; Hahn, Y. K.; Adjan, V. V.; Zou, S.; Buch, S. K.; Nath, A.; Bruce-Kelle, A. J.; Knapp, P. E. HIV-1 tat and morphine have interactive effects on oligodendrocyte survival and morphology. *Glia* **2009**, 57, 194-206.

[8] Kitchen, S. G.; Whitmire, J. K.; Jones, N. R.; Galic, Z.; Kitchen, C. M. R.; Ahmed, R.; Zack, J. A.; Chisari, F. V. The CD4 molecule on CD8+ T lymphocytes directly enhances the immune response to viral and cellular anitgens. *Proc. Natl. Acad. Sci. U.S.A.* **2005**, 102, 3794-3799.

[9] Kileen, N.; Davis, C. B.; Chu, K.; Crooks, M. E. C.; Sawada, S.; Scarborough, J. D.; Boyd, K. A.; Stuart, S. G.; Xu, H.; Littman, D. R. CD4 function in thymocyte differentiation and T cell activation. *Philos. Trans. R. Soc. Lond., B, Biol. Sci.* **1993**, 342, 25-34.

[10] Chan, D. C.; Kim, P. S. HIV entry and its inhibition. *Cell.* **1998**, 93, 681-684.

[11] Greenough, T. C.; Brettler, D. B.; Somasundaran, M.; Panicali, D. L.; Sullivan, J. L. Human immunodeficiency virus type 1- specific cytotoxic T lymphocytes (CTL), virus load, and CD4 T cell loss: evidence supporting a protective role for CTL in vivo. *J. Infect. Dis.* **1997**, 176, 118-125.

[12] Ganusov, V. V.; Neher, R. A.; Perelson, A. S. Mathematical modeling of escape of HIV from cytotoxic T lymphocyte responses. *J. Stat. Mech.* **2013**, 2013, P01010-P01010.

[13] Klein, M. R.; van der Burg, S. H.; Pontesilli, O.; Miedema, F. Cytotoxic T lymphocytes in HIV-1 infection: a killing paradox? *Immun. Today* **1998**, 19, 317-324.

[14] Fryer, H. R.; Frater, J.; Duda, A.; Roberts, M.G.; SPARTAC Trial Inverstigators; Phillips, R. E.; McLean, A. R. Modelling the Evolution and Spread of HIV Immune Escape Mutants. *PloS Pathogens* **2010**, 6.

[15] Ribeiro, R. M.; Chavez, L. L.; Li, D.; Self, S. G.;Perelson, A. S. Estimation of the initial viral growth rate and basic reproductive number during acute HIV-1 infection. *J. Virol.* **2010**, 84, 6096-6102.

[16] Boutwell, C. L.; Rolland, M. M.; Herbeck, J. T.; Mullins, J. I.; Allen, T. M. Viral evolutions and escape during acute HIV-1 infection. *J. Infect. Dis.* **2010**, 202, S309-S314.

[17] McMichael A. J.; Rowland-Jones, S. L. Cellular immune responses to HIV. *Nature* **2001**, 410, 980-987.

[18] Deng, L.; Pertea, M.; Rongvauz, A.; Want, L.; Durand, C. M.; Ghiaur, G.; Lai, J.; McHugh, H. L.; Hao, H.; Margolick, J. B.; Gurer, C.; Murphy, A. J.; Valenzuela, D. M.; Yancopoulus, G. D.; Deeks, S. G.; Stowig, T.; Kumar, P.; Siliciano, J. D.; Salzberg, S. L.; Flavell, R. A.; Shan, L.; Siliciano, R. F. Broad CTL response is required to clear latent HIV-1 due to dominance of escape mutations. *Nature* **2015**, 381-385.

[19] Konrad, B. P.; Vaiyda, N. K.; Smith?, R. J. Modeling mutation to a cytotoxic T-lymphocyte HIV vaccine. *Math. Popul. Stud.* **2011**, 18, 122-149.

[20] Barouch, D. H.; Kunstman, J.; Glowczwskie, J.; Kunstman, K. J.; Egan, M. A.; Peyerl, F. W.; Santra, S.; Kuroda, M. J.; Schmitz, J. E.; Beaudry, K.; Krivulka, G. R.; Lifton, M. A.; Gorgon, D. A.; Wolinsky, S. M.; Letvin, N. L. Viral escape from dominant simian immunodeficiency virus epitope-specific cytotoxic T lymphocytes in DNA-caccinated rhesus monkeys. *J. Virol.* **2003**, 77, 7367-7375.

[21] Noel, R.; Marrero-Otero, Z.; Kumar, R.; Chompre-Gonzalez, G. S.; Verma, A. S.; Kumar, A. Correlation between SIV tat evolution and AIDS progression in cerebrospinal fluid of morphine-dependent and control macaques infected with SIV and SHIV. *Virology* **2006**, 349, 440-452.

[22] Noel, R.; Kumar, A. SIV vpr evolution is inversely related to disease progression in a morphine-dependent rhesus macaque model of AIDS. *Virology* **2007**, 359, 397-404.

[23] Rivera-Amill, V.; Silverstein, P. S.; Noel, R.; Kumar, S.; Kumar, A. Morphine and rapid disease progression in nonhuman primate model of AIDS: Inverse correlation between disease

progression and virus evolution. *J. Neuroimmune Pharmacol* **2014**, 5, 122-132.

[24] Fuggetta, M.P.; Di Francesco, P.; Falchetti. R.; Cottarelli, A.; Rossi, L.; Tricarico, M.; Lanzilli, G. Effect of morphine on cell-mediated immune responses of human lymphocytes against allogeneic malignant cells. *J Exp Clin Cancer Res* **2005**, 24(2), 255-63.

[25] Miyagi, T.; Chuang, L. F.; Doi, R. H.; Carlos, M. P.; Torres, J. V.; Chuang R. Y. Morphine induces gene expression of antiviral CCR5 in human CEMx174 lymphocytes. *J. Biol. Chem.* **2010**, 275, 31305-31310.

[26] Perelson, A. S.; Ribeiro, R. M. Modeling the within-host dynamics of HIV infection. *BMC Biol.* **2013**, 11.

[27] Chubb M. C.; Jacobsen, K. H. Mathematical modeling and the epidemiological research process. *Eur. J. Epidemiol.* **2010**, 25, 13-19.

[28] Conway, J. M.; Perelson, A. S. Post-treatment control of HIV infection. *PNAS,* **2015**, 112, 5467-5472.

[29] Schwartz, E. S.; Biggs, K. R. H.; Bailes, C.; Ferolito, K. A.; Vaidya, N. K. HIV dynamics with immune responses: Perspectives from mathematical modeling. *Curr. Clin. Microbiol. Rep.* **2016**, 3, 216-224.

[30] Vaidya, N. K.; Ribeiro, R. M.; Perelson, A. S.; Kumar, A. Modeling the effects of morphine on simian immunodeficiency virus dynamics. *PloS Comput. Biol.* **2016**, 12, e1005127.

[31] Mutua, J. M.; Perelson, A. S.; Kumar, A.; Vaidya, N. K. Modeling the Effects of Morphine Altered Virus Specific Antibody Responses on HIV/SIV Dynamics. *Sci. Rep* **2019**, 9, 5423.

[32] Ganusov, V. V.; De Boer, R. J. Estimating costs and benefits of CTL escape mutations in SIV/HIV infection. *PloS Comput. Biol.* **2006**, 3, e24.

[33] Ganusov, V. V.; Goonetilleke, N.; Liu, M. K. P.; Ferrari, G.; Shaw, G. M.; McMichael, A. J.; Borrow, P.; Korber, B. T.; Perelson, A. S. Fitness Costs and Diversity of the Cytotoxic T Lymphocyte (CTL) Response Determine the Rate of CTL Escape during Acute and Chronic Phases of HIV Infection. *J. Virol.* **2011**, 85, 10518-10528.

[34] De Boer, R. J.; Perelson, A. S. Target cell limited and immune control models of HIV jnfection: A comparison. *J. Theor. Biol.* **1998**, 190, 201-214.

[35] Vaidya, N.K.; Peter, M. Modeling Intracellular Delay in Within-Host HIV Dynamics Under Conditioning of Drugs of Abuse. *Bull. Math. Biol.* **2021** 83, 81.

[36] Stafford, M. A.; Corey, L.; Cao, Y.; Daar, E. S.; Ho, D. D.; Perelson, A. S. Modeling plasma

virus concentration during primary HIV infection. *J. Theor. Biol.* **2000**, 203, 285-301.

[37] Ramratnam, B.; Bonhoeffer, S.; Binley, J.; Hurley, A.; Zhang, L.; Mittler, J. E.; Markowitz, M.; Moore, J. P.; Perelson, A. S.; Ho, D. D. Rapid production and clearance of HIV-1 and hepatitis C virus assessed by large volume plasma apheresis. *Lancet.* **1999**, 354, 1782.

[38] Mansky, L. M.; Temin, H. M. Lower in vivo mutation rate of human immunodeficiency virus type 1 than that predicted from the fidelity of purified reverse transcriptase. *J. Virol.* **1995**, 69, 5087-5094.

[39] Adams, B. M.; Banks, H. T.; Davidian, M.; Kwon, H.-D.; Tran, H. T.; Wynne, S. N. and Rosenberg, E. S. HIV dynamics: Modeling, data analysis, and optimal treatment protocols. *J. Comput. Appl. Math.* **2005**, 184(1): 10-49.

[40] Tarfulea, N. E. A mathematical model for CTL effect on a latently infected cell inclusive HIV dynamics and treatment. *AIP Conf. Proc.* **2017** 1895(1): 070005.

[41] Olkkola, K. T.; Maunuksela, E.; Korpela, R.; Rosenberg, P. H. Kinetics and dynamics of postoperative intravenous morphine in children. *Clin. Pharmacol. Ther.* **1988**, 44, 128-136.

[42] Castillo-Chavez, C.; Feng, Z.; Huang, W. *Mathematical Approaches for Emerging and Reemerging Infections Diseases: An Introduction,* 1st ed.; Springer-Verlag, New York, 2002, pp. 229-250.

[43] Diekmann, O.; Heesterbeek, J. A. P.; Roberts, M. G. The construction of next-generation matrices for compartmental epidemic models. *J. R. Soc. Interface* **2009**, 7, 873-875.

[44] Marino, S.; Hogue, I. B.; Ray, C. J.; Kirschner, D. E. A methodology for performing global uncertainty and sensitivity analysis in systems biology. *J. Theor. Biol.* **2008**, 254, 178-196.

[45] Perera, S. D.; Perera, S. S. N.; Jayasinghe, S. Modeling and sensitivity of dengue viral dynamics. *Int. J. Curr. Res.* **2006**, 8, 34899-34906.

[46] Rodrigues, H.S.; Monteiro, M. T. T.; Torres, D. F. M. Sensitivity analysis in a dengue epidemiological model. *Conference Papers in Mathematics* **2013**, 2013, 721406.

[47] Perko, L. *Differential equations and dynamical systems*, 2nd ed.; Springer-Verlag, New York, 1991.

[48] Jordan, D. W.; Smith, P. *Nonlinear ordinary differential equations: An introduction to dynamical systems*, 3rd ed.; Oxford University Press, New York, 1999.

[49] Vaidya, V. K.; Rong, L. Modeling pharmacodynamics on HIV latent infection: Choice of drugs is key to successful cure via early therapy. *SIAM J. Appl. Math.* **2017**, 77, 1781-1804.

[50] Kwon, H.-D. Optimal treatment strategies derived from a HIV model with drug-resistant mutants. *Appl. Math. Comput.* **2007**, 188(2): 1193-1204.

Modeling the Effects of Drugs of Abuse on Within-host Dynamics of Two HIV Species

Peter M. Uhl[a,b,c], Naveen K. Vaidya[a,b,c,*]

[a] *Computational Science Research Center, San Diego State University, San Diego, CA, USA*
[b] *Department of Mathematics and Statistics, San Diego State University, San Diego, CA, USA*
[c] *Viral Information Institute, San Diego State University, San Diego, CA, USA*

Abstract

Injection drug use is one of the most significant risk factors associated with contracting human immunodeficiency virus (HIV), and drug users infected with HIV suffer from a higher viral load and rapid disease progression. While replication of HIV may result in many mutant viruses that can escape recognition of the host's immune response, the presence of morphine (a drug of abuse) can decrease the viral mutation rate and cellular immune responses. This study develops a mathematical model to explore the effects of morphine-altered mutation and cellular immune response on the within-host dynamics of two HIV species, a wild-type and a mutant. Our model predicts that the morphine-altered mutation rate and cellular immune response allow the wild-type virus to outcompete the mutant virus, resulting in a higher set point viral load and lower CD4 count. We also compute the basic reproduction numbers and show that the dominant species is determined by morphine concentration, with the mutant dominating below and the wild-type dominating above a threshold. Furthermore, we identified three biologically relevant equilibria, infection-free, mutant-only, and coexistence, which are completely characterized by the fitness cost of mutation, mutant escape rate, and morphine concentration.

Keywords: HIV, mutation, viral escape, morphine

*Corresponding author
5500 Campanile Dr
San Diego, Ca 92182
Email address: nvaidya@sdsu.edu (Naveen K. Vaidya)

1. Introduction

Human immunodeficiency virus (HIV) is a significant health concern worldwide, with 37.7 million infected people globally in 2021 [1]. In addition to sexual contact, HIV transmission is also commonly associated with recreational drug use through needle sharing between drug users [2, 3]. Drug use has also been shown to have several detrimental effects on people infected with HIV, such as a higher viral load, a more rapid progression to AIDS, a greater chance of HIV-related neurological complications, and an overall higher mortality rate [4, 5, 6, 7]. Therefore, it is essential to study how the conditioning of drugs of abuse affects the progression of HIV infections.

HIV replicates within target CD4+ T-cells. Individual virions bind to the target cell membrane, enter the target cell, replicate viral RNA, and then the infected cell releases the newly produced virus into the environment [8, 9, 10]. One of the defense mechanisms the host implements is a cellular immune response in the form of cytotoxic T-lymphocytes (CTLs), which are able to detect and kill infected cells by recognizing epitopes on the surface of infected cells, thereby limiting viral replication [11, 12]. The virus replication process is highly error-prone, resulting in many mutations [13]. Many mutant viruses express epitopes different from wild-type viruses and escape detection by CTLs [10, 13, 14]. Pressure to escape CTLs, combined with the high turnover of virions and infected cells, plays a significant role in allowing HIV to establish infection [15, 16, 17] and poses a major challenge in the control of the infection by immune responses, thereby causing obstacles in developing successful CTL-based vaccines [18, 19, 20].

Animal models with SIV (Simian Immunodeficiency Virus) in rhesus macaques have demonstrated several adverse effects that drugs of abuse can have on the prognosis of infection. In the experiment by Kumar et al. [6], morphine-addicted animals were found to have decreased CD4+ T-cell count and increased set-point viral load compared to non-addicted animals. Many experimental studies have demonstrated the three major effects of drugs of abuse on the dynamics of HIV/SIV: (i) Drugs of abuse have been shown to increase expression of the CCR5 co-receptor in target cells, making them more susceptible to infection [5, 6, 25]; (ii) Opiates are known to diminish cellular immune responses [23, 24]; and (iii) the conditioning of the drugs of abuse is negatively correlated with SIV viral evolution and disease progression [21, 22, 23], indicating a lower mutation rate in the presence of drugs of abuse. While there is ample experimental evidence for these effects, their quantitative understanding is minimal. Therefore, the potential combined alteration in mutation, immune response, and cell susceptibility due to drugs of abuse need to be considered to quantify

the effects of opiate use on HIV infections.

Mathematical models have been previously used to study infectious diseases, including HIV/SIV [12, 19, 26, 27, 28, 29, 30, 31, 32, 33]. Models have also been developed to investigate viral escape [32, 33, 12], antibody responses [31], and viral evolution [19]. In this study, we present a mathematical model of HIV infection that incorporates morphine effects on the dynamics of viral replication, cellular immune responses, and mutation. We analyze the model to determine how morphine affects viral mutation and the long-term dynamics of mutant and wild-type virus species. We were able to fully characterize the dynamics using three steady-state solutions of the model: an infection-free steady state, a mutant-only steady state, and a coexistence steady state. Furthermore, we were able to show that the concentration of morphine present within the host is critical for the stability of the steady states of the virus-immune dynamical system.

2. Method

2.1. Mathematical model

2.1.1. Virus-cell dynamics

We extend the standard HIV dynamics model [26, 29] to include morphine effects on target cell susceptibility, viral mutation, and cellular immune response, which have been established in various experimental studies [5, 6, 21, 22, 23, 24, 25]. Following Vaidya et al. [30, 31], we include two populations of CD4+ target cells based on levels of CCR5 co-receptor expression: a population with lower susceptibility to infection, T_l, and a population with higher susceptibility to infection, T_h [5, 6, 25]. The viral mutation is modeled by including two viral species, a wild-type virus, V_w, and a mutant virus, V_m [13, 17]. We assume free virus particles infect target cells, resulting in corresponding infected cell populations, I_w and I_m. Cellular immune responses are represented by a population of CTLs, denoted by C, which directly kills infected cells [19, 34].

Target cells are recruited at a constant rate λ and are assumed to belong to the T_l population. Target cells switch from T_l to T_h at rate r and from T_h to T_l at rate q [30]. Both populations of target cells die at per capita rate δ_T [26, 29]. Target cells in the T_l population are infected by the wild-type virus at rate β_l and by the mutant virus at a rate $(1-F)\beta_l$, where F denotes the fitness cost of mutation, with $0 \leqslant F \leqslant 1$. Note that we assume the mutant virus to have a lower infection rate than the wild-type virus [33]. Similarly, T_h cells are infected at rates β_h and $(1-F)\beta_h$ by the

wild-type and mutant viruses, respectively. Due to mutation, a fraction ϵ of target cells infected by wild-type virus become mutant-infected cells, and the remaining $(1-\epsilon)$ stay wild-type infected cells [19].

Both virus species are produced by their corresponding infected cell population at rate p per cell and are cleared at rate δ_V [19]. We consider only forward mutation, i.e., target cells infected by the mutant virus do not revert to the wild-type infected population because the back mutation in the presence of morphine is not understood well. Wild-type infected cells, I_w, are killed by CTLs at rate b. Due to responses by epitope-specific CTLs, there is a reduced recognition of mutant-infected cells by the host's immune responses [19, 20]. We interpret this reduced rate as the escape rate. CTLs kill I_m cells at rate $\frac{b}{1+B}$, in which the base CTL killing rate b is reduced by the mutant escape ratio $1+B$. The mutant escape rate, $B>0$, represents a reduction in the ability of the host's cellular immune response to kill cells infected by the mutant virus compared to cells infected by the wild-type virus. Both classes of infected cells die at per capita rate δ_I. CTLs are produced at rate α per infected cell [19, 34], die at rate δ_C, and recruited at a constant rate ω [28], which also includes background production other than those proportional to infected cells.

2.1.2. Effects of morphine

Based on experimental results, we include the effects of morphine through three mechanisms: the higher transfer of T_l cells into T_h cells due to increased co-receptor expression [6, 25], the decrease in viral mutation [21, 22], and the decrease in CTL production [23]. We, therefore, make the transition parameters r and q morphine-dependent, i.e., $r=r(M)$ and $q=q(M)$, where M is the concentration of morphine. Since it is expected that $r(M)$ is an increasing function of morphine and $q(M)$ is a decreasing function of morphine, we model $r(M)$ and $q(M)$ using an E_{max} model as done previously [35],

$$\begin{aligned} r(M) &= r_c + (r_m - r_c)\eta_r(M), \\ q(M) &= q_m + (q_c - q_m)\eta_q(M), \end{aligned} \tag{1}$$

where

$$\begin{aligned} \eta_r(M) &= \frac{M^n}{M_h^n + M^n}, \\ \eta_q(M) &= 1 - \eta_r(M). \end{aligned} \tag{2}$$

Here, r_c and r_m are the minimum and maximum values of $r(M)$, q_c and q_m are the minimum and maximum values of $q(M)$, n is Hill's coefficient for the E_{max} model, and M_h is the morphine concentration that gives $r(M)$ and $q(M)$ the value half-way between their respective minimums and maximums. Since morphine causes a decrease in viral mutation [21, 22], we model the mutation rate as $\frac{\epsilon}{\mu+\eta M}$, where μ and η are parameters related to the effect of morphine on mutation. To model the decrease in CTL production due to morphine, we take the CTL recruitment rate as $\omega e^{-\psi M}$ and the CTL production rate in response to infection as $\frac{\alpha}{\gamma+\xi M}$, where ψ, γ, and ξ are parameters related to the decrease in CTL production due to morphine. The full model is given by the following seven-dimensional system of ODEs:

$$
\begin{aligned}
\frac{dT_l}{dt} &= \lambda + \left(q_m + (q_c - q_m)\left(1 - \frac{M^n}{M_h^n + M^n}\right)\right) T_h - \left(r_c + (r_m - r_c)\frac{M^n}{M_h^n + M^n}\right) T_l \\
&\quad - \beta_l V_w T_l - (1-F)\beta_l V_m T_l - \delta_T T_l, \\
\frac{dT_h}{dt} &= \left(r_c + (r_m - r_c)\frac{M^n}{M_h^n + M^n}\right) T_l - \left(q_m + (q_c - q_m)\left(1 - \frac{M^n}{M_h^n + M^n}\right)\right) T_h \\
&\quad - \beta_h V_w T_h - (1-F)\beta_h V_m T_h - \delta_T T_h, \\
\frac{dV_w}{dt} &= pI_w - \delta_V V_w, \\
\frac{dV_m}{dt} &= pI_m - \delta_V V_m, \\
\frac{dI_w}{dt} &= \left(1 - \frac{\epsilon}{\mu + \eta M}\right)(\beta_l V_w T_l + \beta_h V_w T_h) - bI_w C - \delta_I I_w, \\
\frac{dI_m}{dt} &= \frac{\epsilon}{\mu + \eta M}(\beta_l V_w T_l + \beta_h V_w T_h) + (1-F)(\beta_l V_m T_l + \beta_h V_m T_h) - \frac{b}{1+B} I_m C - \delta_I I_m, \\
\frac{dC}{dt} &= \omega e^{-\psi M} + \frac{\alpha}{\gamma + \xi M}(I_w + I_m) C - \delta_C C.
\end{aligned}
\tag{3}
$$

A schematic diagram of the model is shown in Figure 1.

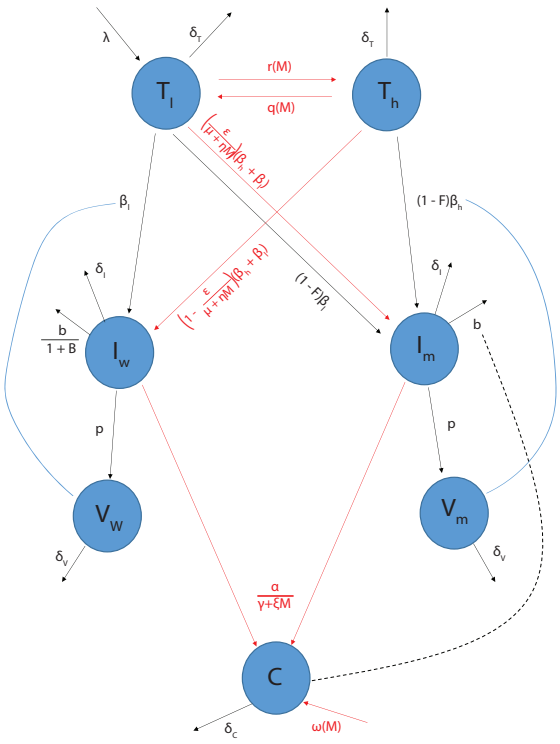

Figure 1: Schematic diagram of the model. The model includes two populations of target cells distinguished by susceptibility to infection, two viral strains and corresponding infected populations, and a cellular immune response in the form of CTLs. Viral species are distinguished by their infectivity rates and ability to escape from immune responses. Mechanisms that are affected by morphine, shown by red arrows, are the rate of viral mutation, target cell susceptibility, and production rate of CTLs.

2.2. Parameter estimation

We obtained some parameters from the literature and estimated some parameter values based on previously published studies. Following Vaidya et al. [30], we assume 10^6 target cells per ml of blood, with 40980 cells/ml belonging to the T_h population and the remaining 959020 cells/ml to the

T_l population. We assume that the infection begins with free virus only, and there are no infected cells, so we take $I_w(0), I_m(0) = 0$. Also, as described in Vaidya et al. [30], the SIV infection was established with 3×10^5 RNA copies of the virus. Assuming a macaque contains approximately 1.5 liters of extracellular water, we can estimate $V_0 = \frac{3 \times 10^5}{1.5L} \approx 200$ viral RNA copies/ml [30], which we assume to belong entirely to the V_w population. Estimates for $\lambda, \beta_l, \beta_h, r_c, r_m, q_m, q_c$, and δ_I were taken from Vaidya et al. [30], where these values were obtained by fitting the model to experimental data. In particular, they estimated β_h to be approximately two orders of magnitude higher than β_l. The viral production rate, p, is estimated from the SIV *in vivo* burst size in rhesus macaques and the average life span of an infected cell, giving $p = 2500$ per cell/day [30].

Based on modeling work by Stafford et al. [36], we take $\delta_T = 1/100 = 0.01$ per day, corresponding to a target cell life span of 100 days. Ramratnam et al. [37] give an estimated range of HIV viral clearance between 9.1 and 36 virions per day, so we use their average of 23 virions per day as our base value for δ_V. Mansky and Temin [38] determined the *in vivo* mutation rate of HIV-1 to be 3.4×10^{-5} mutations per base pair per generation, so we take the mutation rate $\epsilon = 3 \times 10^{-5}$. Following De Boer and Perelson [34], we take $\delta_C = 0.2$ per day as an estimate for the turnover of CTLs and $\alpha/\gamma = 6.7 \times 10^{-5}$ for the infected cell-dependent CTL production rate. Similar to other modeling works, we also include a constant production of CTLs $\omega = 15$ to include potential background production other than those proportional to infected cells [28, 39, 40].

Previous work by Ganusov et al. [33] investigated the rate of escape by mutant viruses from CTL responses. They measured the rate of escape by a single mutant variant as the average difference between the rate of mutant killing by CTLs and the production rate of the mutant. They consider the range of killing of infected cells (wild-type and mutant) by CTLs to be 0.01-0.5 per day, so we take $b = 0.25$ per day as our base value. In their study, the upper-value $b = 0.5$ corresponds to a wild-type virus, and the lower-value $b = 0.01$ to an escape mutant. Noting that $\frac{0.5}{0.01} = 50$, we will vary the escape ratio, B, from 0 to 50 with $B = 30$ as our base value [33].

In an experiment performed on children aged between two and six years, Olkkola et al. [41] observed initial morphine concentrations between 28 and 325 ug/l of blood plasma. To include this range, we will consider values of M to be between 0 and 200 ug/l [41]. Accordingly, we take $M_h = 100$, corresponding to the half-saturation value of $r(M)$ and $q(M)$. The estimated parameters and their descriptions are summarized in Table 1.

Table 1: Parameter Values

Parameter	Value (Range for LHS)	Description	Reference
λ	3690 (1500, 10000) ml/day	Production rate of T_l cells	[30]
$r(M)$	$r_c + (r_m - r_c)\eta_r(M)$ $(0.005, 2.7)$	Transition rate from T_l to T_h	[30]
$q(M)$	$q_c + (q_m - q_c)\eta_q(M)$ $(10^{-8}, 2.8)$	Transition rate from T_h to T_l	[30]
r_c	0.16 day^{-1}	Minimum value of r	[30]
r_m	0.52 day^{-1}	Maximum value of r	[30]
q_c	1.23×10^{-6} day^{-1}	Minimum value of q	[30]
q_m	0.25 day^{-1}	Maximum value of q	[30]
M_h	100 ug/l	Half morphine value for $r(M), q(M)$	[41]
n	8	Hill's coefficient of morphine response	[30]
β_l	10^{-9} $(10^{-11}, 10^{-5})$ ml/day	Wild- type infection rate of T_l cells	[30]
β_h	10^{-7} $(10^{-9}, 10^{-3})$ ml/day	Wild -type infection rate of T_h cells	[30]
F	0.1 $(0 - 1)$	Fitness cost of mutation	Assumed
p	2500 $(500, 5500)$ day^{-1}	Production rate of virus	[30]
b	0.25 $(0.005, 1.8)$ ml/day	CTL killing rate of wild-type	[33]
B	30 $(0.1, 100)$	Mutant escape ratio	Assumed
α	6.7×10^{-5} ml/day	CTL response to infection	[34]
γ	1	Morphine effect on α	Assumed
ξ	1 l/ug	Morphine effect on α	Assumed
ω	15 $(0.001, 40)$ ml/day	Base CTL production rate	Assumed
ψ	0.1 $(0.001, 1.5)$ ml/day	CTL prduction decay rate	Assumed
ϵ	3×10^{-5} $(3 \times 10^{-7}, 3 \times 10^{-3})$	Mutation rate	[38]
μ	1 $(0.01, 50)$	Morphine effect on ϵ	Assumed
η	1 $(0.01, 50)$ l/ug	Morphine effect on ϵ	Assumed
δ_T	0.01 $(0.001, 1.2)$ day^{-1}	Target cell death rate	[36]
δ_V	23 $(1, 50)$ day^{-1}	Virus clearance rate	[37]
δ_I	0.7 $(0.01, 10)$ day^{-1}	Infected cell death rate	[30]
δ_C	0.2 $(0.001, 1.6)$ day^{-1}	CTL death rate	[34]
M	$0 - 200$ ug/l	Concentration of morphine	[41]

3. Results

3.1. Basic reproduction number

The basic reproduction number, denoted by R_0, is defined as the average number of secondary infected cells resulting from a single initial infected cell when target cells are not limited [42]. R_0 is an important quantity in the study of viral dynamics that provides a threshold condition for infection to persist ($R_0 > 1$) and to die out ($R_0 < 1$).

We use the next-generation matrix method [43] to obtain an expression for the basic reproduction number of our model. The next-generation matrix is obtained from the infected subsystem of the model, i.e., the equations of the system corresponding to viruses and infected cells [43]. For our model, the infected subsystem is given by

$$\begin{aligned}
\frac{dV_w}{dt} &= pI_w - \delta_V V_w, \\
\frac{dV_m}{dt} &= pI_m - \delta_V V_m, \\
\frac{dI_w}{dt} &= (1-\hat{\epsilon}(M))(\beta_l V_w T_l + \beta_h V_w T_h) - bI_w C - \delta_I I_w, \\
\frac{dI_m}{dt} &= \hat{\epsilon}(M)(\beta_l V_w T_l + \beta_h V_w T_h) + (\hat{\beta}_l V_m T_l + \hat{\beta}_h V_m T_h) - \frac{b}{1+B} I_m C - \delta_I I_m,
\end{aligned} \tag{4}$$

where $\hat{\epsilon}(M) = \frac{\epsilon}{\mu+\eta M}$, $\hat{\beta}_l = (1-F)\beta_l$, and $\hat{\beta}_h = (1-F)\beta_h$. The infection-free equilibrium (IFE) is the steady-state solution of the model, in which all infected cell and virus populations are zero. For our model, we compute the IFE as $(T_l^*, T_h^*, 0, 0, 0, 0, C^*)$, where

$$\begin{aligned}
T_l^* &= \frac{\lambda(q(M)+\delta_T)}{\delta_T(q(M)+r(M)+\delta_T)}, \\
T_h^* &= \frac{\lambda r(M)}{\delta_T(q(M)+r(M)+\delta_T)}, \\
C^* &= \frac{\hat{\omega}(M)}{\delta_C},
\end{aligned} \tag{5}$$

and $\hat{\omega}(M) = \omega e^{-\psi M}$. Now, we linearize the infected subsystem about the IFE and decompose it into $\mathcal{F} - \mathcal{V}$, where $\mathcal{F}$ is the part of the system that describes newly infected components, and $\mathcal{V}$ is the part that describes transitions of cells and viruses in and out of compartments. $\mathcal{F}$ and $\mathcal{V}$ for

our model are given by

$$\mathcal{F} = \begin{bmatrix} 0 & 0 & 0 & 0 \\ 0 & 0 & 0 & 0 \\ (1-\hat{\epsilon}(M))(\beta_l T_l^* + \beta_h T_h^*) & 0 & 0 & 0 \\ \hat{\epsilon}(M)(\beta_l T_l^* + \beta_h T_h^*) & (\hat{\beta}_l T_l^* + \hat{\beta}_h T_h^*) & 0 & 0 \end{bmatrix} \tag{6}$$

and

$$\mathcal{V} = \begin{bmatrix} \delta_V & 0 & -p & 0 \\ 0 & \delta_V & 0 & -p \\ 0 & 0 & \delta_I + bC^* & 0 \\ 0 & 0 & 0 & \delta_I + \frac{b}{1+B}C^* \end{bmatrix}. \tag{7}$$

The next-generation matrix is $\mathcal{F}\mathcal{V}^{-1}$ [43]. The basic reproduction number of our model is then obtained as the spectral radius of $\mathcal{F}\mathcal{V}^{-1}$, i.e., $R_0 = \sigma(\mathcal{F}\mathcal{V}^{-1}) = \max\{R_0^w, R_0^m\}$, where

$$\begin{aligned} R_0^w &= \frac{(1-\hat{\epsilon}(M))(\beta_h T_h^* + \beta_l T_l^*)p}{\delta_V(bC^* + \delta_I)} \quad \text{and} \\ R_0^m &= \frac{(1-F)(\beta_h T_h^* + \beta_l T_l^*)(1+B)p}{\delta_V(\delta_I B + bC^* + \delta_I)} \end{aligned} \tag{8}$$

represent the basic reproduction number corresponding to the wild-type and mutant virus, respectively. Note that since $\hat{\epsilon}(M), T_l^*, T_h^*$, and C^* are morphine dependent, R_0^w and R_0^m are also morphine dependent. In addition, if $R_0^w < 1$ and $R_0^m < 1$ the infection will die out while if either $R_0^w > 1$ or $R_0^m > 1$ the infection will be established [42]. Using the parameter values in Table 1, we compute $R_0^w = 0.08$, $R_0^m = 1.07$, and $R_0 = max\{R_0^w, R_0^m\} = 1.07 > 1$, indicating that the infection persists for this basic parameter set.

To study the effect of each parameter on R_0, we first determine the local sensitivity of R_0^w and R_0^m to changes in individual parameters. For a parameter ρ of the model, the forward sensitivity index is given by

$$S_\rho = \frac{\rho}{R_0}\frac{\partial R_0}{\partial \rho}. \tag{9}$$

Then S_ρ determines the relative instantaneous change in R_0 caused by a change in ρ [44, 45, 46]. The higher the values of S_ρ, the more sensitive R_0 is to ρ. Also, positive (negative) values of S_ρ

indicate that R_0 increases (decreases) as ρ increases. Sensitivity indices for R_0^w and R_0^m are shown in Figure 2 (left). We found that R_0^w and R_0^m are positively correlated to λ, r, p, and δ_C, indicating that an increase in these parameters is favorable for an infection to occur. This is expected since increasing λ, r, and δ_C will result in more (susceptible) target cells available for infection while increasing p results in more virions that can infect target cells. On the other hand, R_0^w and R_0^m are negatively correlated to q, b, δ_T, δ_V, and ω. Increased δ_T and δ_V cause increased death of target cells and viral clearance, respectively, both unfavorable for the virus, while a larger ω means more CTLs are responding to the infection. Larger values of parameter q increase target cells in the lower susceptibility population, and increased CTL killing rate b indicates a stronger immune response. Both of these mechanisms are also unfavorable to the virus. In addition, R_0^m is positively related to B and negatively related to F since a mutant virus benefits from a higher rate of immune escape and lower fitness of mutation. We found that R_0^w and R_0^m are less sensitive to changes in β_l, β_h, ϵ, μ, η or ψ on these base-case parameters.

To further quantify the global sensitivity of R_0^w and R_0^m to the parameters, we used Latin hypercube sampling (LHS) to obtain 10,000 samples of parameter sets. We used these parameters to calculate corresponding R_0^w and R_0^m values. In LHS, individual parameter values were sampled uniformly from the interval $[\rho_{min}, \rho_{max}]$ for each parameter ρ, where ρ_{min} and ρ_{max} were selected to give a realistic range of values (Table 1). The PRCCs of rank-transformed data were then calculated as the Pearson correlation coefficient between the vectors of selected values and the reproductive numbers [44].

The obtained partial rank correlation coefficients are shown in Figure 2 (right). The LHS-based sensitivities are consistent with the forward sensitivity indices, but the magnitude of sensitivity is relatively lower in general. Here also, λ, r, p, and δ_C, i.e., those related to increased amounts of virus and susceptible target cells, are mostly associated with more infectious viruses. Similarly, higher values of the CTL killing rate b, death rates $\delta_T, \delta_V, \delta_I$, and CTL production rate ω lead to more viruses. Note that R_0^w is unaffected by changes in F and B since these parameters only relate to the viability of the mutant virus. The mutant benefits from a low fitness cost and high rate of immune escape, which is reflected in R_0^m being positively associated with B and negatively associated with F.

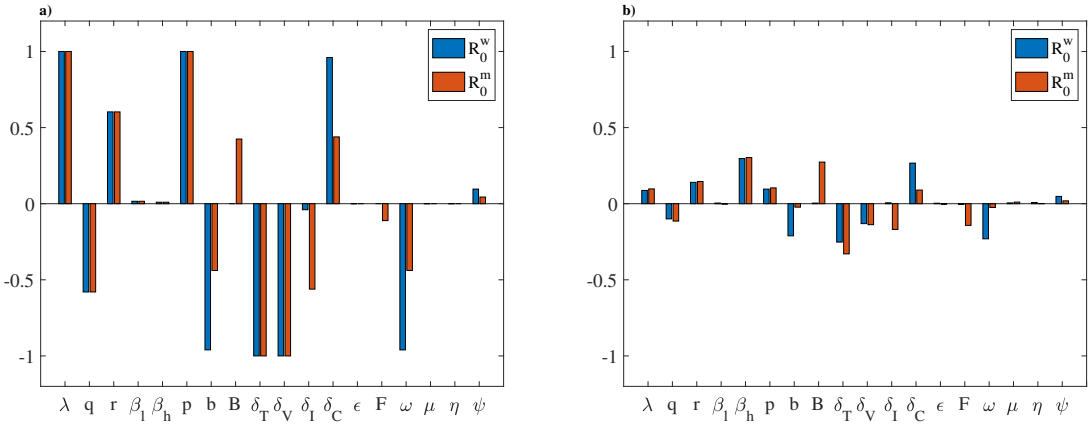

Figure 2: Local sensitivity indices (left) and partial rank correlation coefficients from 10,000 LHS for R_0^w and R_0^m. A positive value is favorable to the virus infection while a negative value is unfavorable to the viral infection. The higher the magnitude of the sensitivity value, the more sensitive R_0 is to the parameter.

3.2. Virus species switch

The viral species with a larger reproduction number can be considered to be the dominant species. For the base case with $M = 0$ we obtained $R_0^w = 0.08$ and $R_0^m = 1.07$, indicating that the mutant is the dominant viral population. An increase in M increases both R_0^w and R_0^m, and so R_0. For example, $M = 200$ causes R_0^w, R_0^m, and R_0 to become 5.6, 5.05, and 5.6, respectively. We found that increasing the amount of morphine past a threshold value, M_{thresh}, results in a viral species switch. The wild-type becomes the dominant viral population when the morphine concentration exceeds M_{thresh} (Figure 3).

The value of M_{thresh} can be determined by solving $R_0^w(M) = R_0^m(M)$ for M. For $M < M_{thresh}$, the mutant dominates, and for $M > M_{thresh}$, the wild-type dominates. Due to the nonlinearity in R_0^w and R_0^m, we did not find a closed form for M_{thresh} and obtained it numerically. For our base parameter values, $M_{thresh} \approx 54$, the wild-type is the dominant population for $M > 54$, and the mutant dominates for $M < 54$.

We now evaluate the effect of F (fitness cost) and B (immune escape) on M_{thresh}. As predicted by our model (Figure 3), in general, M_{thresh} decreases as F increases and/or B decreases. For a substantially higher fitness cost (for example, $F > 0.93$ in our computations), the mutant population is not fit enough to out-compete the wild-type, and the wild-type always dominates for any values

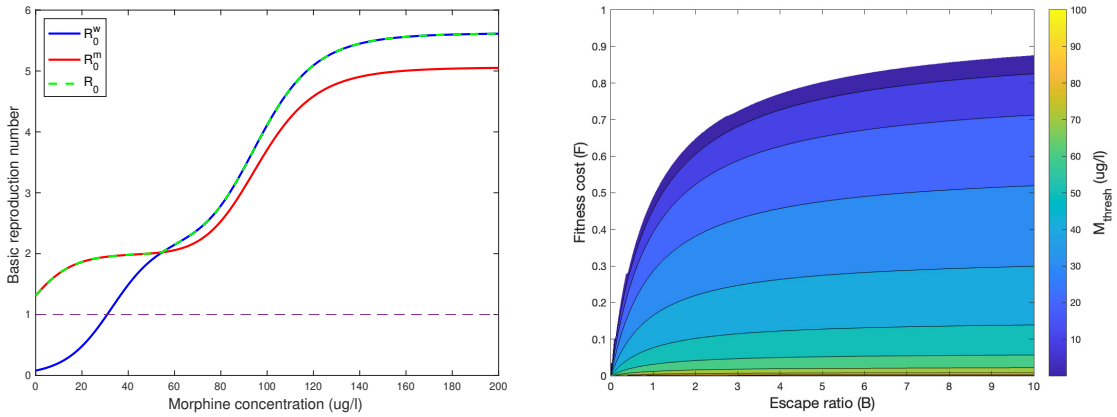

Figure 3: (Left) R_0^w and R_0^m as functions of M. With parameter values as in Table 1, $M_{thresh} \approx 54$ ug/ml. The mutant is the dominant population for $M < 54$ ug/ml and the wild-type is dominant for $M > 54$ ug/ml. (Right) M_{thresh} in $F - B$ parameter space. An increase in fitness cost (F) or a decrease in escape ratio B causes an increase in M_{thresh} value. The upper-left region represents (F, B) values that cause the wild-type to always dominate.

of M. On the other hand, for a low enough B ($B < 0.12$ in our computations), we did not find any value of M_{thresh} because CTLs are highly effective against the mutant virus, and the mutant virus cannot out-compete the wild-type virus.

3.3. Stability of steady-states

3.3.1. Infection-free equilibrium

The IFE is shown in Section 3.1. As discussed earlier, the local stability of the IFE is determined by the basic reproduction number. It is easy to prove that the IFE is locally asymptotically stable if $R_0 < 1$ and unstable if $R_0 > 1$ [42].

3.3.2. Wild-type only equilibrium

A wild-type only equilibrium is a solution, $(T_l^*, T_h^*, V_w^*, 0, I_w^*, 0, C^*)$, of the following system of equations

$$\begin{aligned}
0 &= \lambda + q(M)T_h^* - r(M)T_l^* - \beta_l V_w^* T_l - \delta_T T_l^*, \\
0 &= r(M)T_l^* - q(M)T_h^* - \beta_h V_w^* T_h^* - \delta_T T_h^*, \\
0 &= pI_w^* - \delta_V V_w^*, \\
0 &= (1-\hat{\epsilon}(M))(\beta_l V_w^* T_l + \beta_h V_w^* T_h^*) - bI_w^* C^* - \delta_I I_w^*, \\
0 &= \hat{\epsilon}(M)(\beta_l V_w^* T_l^* + \beta_h V_w^* T_h^*), \\
0 &= \hat{\omega}(M) + \hat{\alpha}(M) I_w^* C - \delta_C C^*.
\end{aligned} \tag{10}$$

Solving the second equation for T_h^* gives:

$$T_h^* = \frac{r(M)}{q(M) + \beta_h V_w^* + \delta_T} T_l^*, \tag{11}$$

and, since $\hat{\epsilon}(M) \neq 0$, the fifth equation is equivalent to

$$0 = \beta_l V_w^* T_l^* + \beta_h V_w^* T_h^*. \tag{12}$$

This implies $V_w^* = 0$, which corresponds to the IFE, or

$$0 = T_l^* \Big(\beta_l + \beta_h \Big(\frac{r(M)}{q(M) + \beta_h V_w^* + \delta_T} \Big) \Big). \tag{13}$$

Then either $T_l^* = 0$ or $\beta_l + \beta_h(\frac{r(M)}{q+\beta_h V_w^* + \delta_T}) = 0$. Substituting $T_l^* = 0$ into the first equation gives the negative solution $T_h^* = -\frac{\lambda}{q(M)}$. Also, letting $\beta_l + \beta_h(\frac{r(M)}{q(M)+\beta_h V_w^* + \delta_T}) = 0$, we get

$$V_w^* = -\frac{1}{\beta_h} \Big(\frac{\beta_h r(M)}{\beta_l} + q(M) + \delta_T \Big), \tag{14}$$

which is also a negative solution. Therefore, the system does not provide a wild-type only equilibrium. This is expected because the wild-type virus promotes a fraction of infections transitioned to the mutant population due to mutation.

3.3.3. Mutant-only equilibrium

The mutant only equilibrium (MOE) is the steady-state solution of the model, in which only the mutant population exists. The MOE of our model takes the form $(\hat{T_l}, \hat{T_h}, 0, \hat{V_m}, 0, \hat{I_m}, \hat{C})$, where

$$\begin{aligned}
\hat{T_h} &= \frac{r(M)\lambda}{(q(M)+\hat{\beta}_h\hat{V}_m+\delta_T)(r(M)+\hat{\beta}_l\hat{V}_m+\delta_T)-r(M)q(M)},\\
\hat{T_l} &= \frac{\lambda(q(M)+\hat{\beta}_h\hat{V}_m+\delta_T)}{(q(M)+\hat{\beta}_h\hat{V}_m+\delta_T)(r(M)+\hat{\beta}_l\hat{V}_m\delta_T)-r(M)q(M)},\\
\hat{I_m} &= \frac{\delta_V\hat{V}_m}{p},\\
\hat{C} &= \frac{\hat{\omega}(M)}{\delta_C-\hat{\alpha}\frac{\delta_V\hat{V}_m}{p}},
\end{aligned} \tag{15}$$

and $\hat{V}_m$ is the solution of

$$g(\hat{V}_m) = 0, \tag{16}$$

with

$$\begin{aligned}
g(\hat{V}_m) = &\frac{\hat{\beta}_l\hat{V}_m\lambda\left(\hat{V}_m\hat{\beta}_h+q(M)+\delta_T\right)+\hat{\beta}_h r(M)\hat{V}_m\lambda}{\left(\hat{V}_m\hat{\beta}_h+q(M)+\delta_T\right)\left(\hat{V}_m\hat{\beta}_l+r(M)+\delta_T\right)-r(M)q(M)}\\
&-\frac{b\delta_V\hat{V}_m\hat{\omega}}{(1+B)\,p\left(\delta_C-\frac{\hat{\alpha}\delta_V V_m^*}{p}\right)}-\frac{\delta_I\delta_V\hat{V}_m}{p}.
\end{aligned}$$

Clearly, $\hat{V}_m = 0$ is a solution that corresponds to the IFE. We now obtain solutions with $\hat{V}_m > 0$. We can obtain a value for $\hat{V_m}$ by solving (1) numerically, and substituting into the expressions for $\hat{T_h}, \hat{T_l}, \hat{I_m}$, and $\hat{C}$. Geometrically, $\hat{V_m}$ can be represented by the intersection of the curve $g(\hat{V}_m)$ and the axis $g = 0$. As shown in Figure 4a, the steady-state value of $\hat{V}_m$ at the MOE is the x-intercept of the curve $g(\hat{V}_m)$. We observe that the higher morphine concentrations intersect the x-axis further to the right. These $\hat{V}_m$ values at MOE can be substituted into the expressions for the other variables at MOE. A graph of $\hat{V}_m$ as a function of M (Figure 4b) shows that increasing M causes a larger non-zero equilibrium value of $\hat{V_m}$, indicating a higher set point viral load for larger morphine concentrations, consistent with experimental data [6]. Moreover, increasing M reduces values of T_l, T_h, and C, and increases the value of I_m at the MOE (Figure 4c-f)). Combining all

these results, we conclude that morphine causes infection of more target cells and less killing of infected cells by CTLs at the MOE.

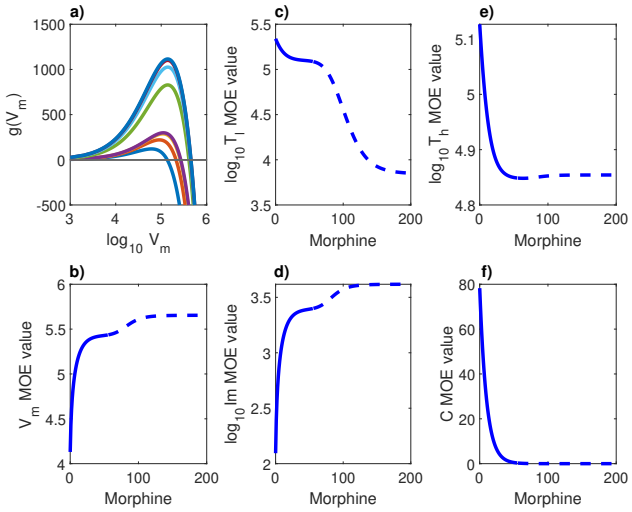

Figure 4: (a) Graphs of $g(V_m)$ (Eq. 16) for different morphine levels. Each color represents a different value of M, and the x-intercept of each curve represents the steady-state viral load at the MOE. (b - f) V_m, T_l, T_h, I_m, and C steady-state values at MOE. Morphine is varied along the x-axis, and the y-axis represents the steady-state value at the MOE. The solid portion of each curve represents locally-stable equilibria, and the dashed portions represent unstable equilibria.

To determine the local stability of the MOE, we calculate the eigenvalues of the Jacobian matrix, J, of the model evaluated at the MOE, given by

$$J = \begin{bmatrix} J_{11} & J_{12} & J_{13} & J_{14} & 0 & 0 & 0 \\ J_{21} & J_{22} & J_{23} & J_{24} & 0 & 0 & 0 \\ 0 & 0 & J_{33} & 0 & J_{35} & 0 & 0 \\ 0 & 0 & 0 & J_{44} & 0 & J_{46} & 0 \\ J_{51} & J_{52} & J_{53} & 0 & J_{55} & 0 & J_{57} \\ J_{61} & J_{62} & J_{63} & J_{64} & 0 & J_{66} & J_{67} \\ 0 & 0 & 0 & 0 & J_{75} & J_{76} & J_{77} \end{bmatrix}, \tag{17}$$

where

$$
\begin{aligned}
J_{11} &= -r(M) - \beta_l V_w - \hat{\beta}_l V_m - \delta_T, & J_{52} &= (1-\hat{\epsilon}(M))\beta_h V_w,\\
J_{12} &= q(M), & J_{53} &= (1-\hat{\epsilon}(M))(\beta_l T_l + \beta_h T_h),\\
J_{13} &= -\beta_l T_l, & J_{55} &= -bC - \delta_I,\\
J_{14} &= -\hat{\beta}_l T_l, & J_{57} &= -bI_w,\\
J_{21} &= r(M), & J_{61} &= \hat{\epsilon}(M)(\beta_l V_w + \hat{\beta}_l V_m),\\
J_{22} &= -q(M) - \beta_h V_w - \hat{\beta}_h V_m - \delta_T, & J_{62} &= \hat{\epsilon}(M)\beta_h V_w + \hat{\beta}_h V_m,\\
J_{23} &= -\beta_h T_h, & J_{63} &= \hat{\epsilon}(M)(\beta_l T_l + \beta_h T_h),\\
J_{24} &= -\hat{\beta}_h T_h, & J_{64} &= \hat{\beta}_l T_l + \hat{\beta}_h T_h,\\
J_{33} &= -\delta_V, & J_{66} &= -\tfrac{b}{1+B}C - \delta_I,\\
J_{35} &= p, & J_{67} &= -\tfrac{b}{1+B}I_m,\\
J_{44} &= -\delta_V, & J_{75} &= \hat{\alpha}(M)C,\\
J_{46} &= p, & J_{76} &= \hat{\alpha}(M)C,\\
J_{51} &= (1-\hat{\epsilon})\beta_l V_w, & J_{77} &= \hat{\alpha}(M)(I_w + I_m) - \delta_C.
\end{aligned}
$$

The MOE is locally asymptotically stable if the real part of each eigenvalue of J is negative and unstable otherwise [47, 48]. We determined the stability of the MOE by computing the eigenvalues of $J(MOE)$ for $M \in [0, 200]$. We observed that each eigenvalue of $J(MOE)$ had a negative real part for $M < M_{thresh}$ and that the real part of one eigenvalue became positive for $M > M_{thresh}$, indicating that the MOE becomes unstable for larger morphine concentrations. This is consistent with the viral species switch presented in Section 3.2, in which the larger values of M allow the wild-type virus to dominate.

3.3.4. Coexistence equilibrium

Due to the model's non-linear nature, we could not obtain an analytical expression for the coexistence equilibrium. However, by examining eigenvalues numerically, we determined that the coexistence equilibrium is locally asymptotically stable when $M > M_{thresh}$. A high morphine concentration (larger than M_{thresh}) allows the wild-type virus to dominate, in which case a small amount of mutant persists due to mutation, resulting in a coexistence equilibrium.

3.3.5. Parameter space and stability for equilibrium

In this section, we numerically investigate the effects of F (mutant fitness cost) and B (immune escape rate) on the stability of the model equilibria by examining R_0^w and R_0^m under the conditioning

of various morphine (M) levels. The stability regions in the $M-F$ and $M-B$ planes are presented in Figure 5. Depending on the combination of M, F, and B, the model evolves to one of the three biologically relevant equilibria based on local stability analysis: (a) If $R_0^w < 1$ and $R_0^m < 1$, the model converges to the IFE; (b) If $R_0^w < 1$ and $R_0^m > 1$, the model converges to the MOE; and (c) If $R_0^w > 1$ and $R_0^w > R_0^m$, the model converges to the coexistence equilibrium (CE).

In Figure 5(left) we present the region in the $M-F$ plane, at which each equilibrium is stable. It is interesting to note that the IFE-MOE and MOE-CE boundaries are quite nonlinear. We observe that a lower fitness cost and lower morphine concentration can cause the MOE to be stable. Similarly, a higher fitness cost and lower morphine concentration result in the stability of infection-free equilibrium. For a substantially higher morphine concentration, the coexistence equilibrium becomes stable regardless of fitness cost, promoting both virus species to survive in the system.

In Figure 5(right), we present the region in the $M-B$ plane for the stability of each equilibrium. In this case, the boundary between the IFE-MOE and MOE-CE is nonlinear, and there is no boundary separating the IFE and CE. As predicted by our model, a smaller B and a lower morphine concentration allow the IFE to become stable. However, a higher B causes the MOE to be stable at a lower level of morphine concentration. Regardless of the escape ratio B, sufficiently high morphine concentration implies the stability of coexistence equilibrium, and both viruses survive in the system.

In summary, a high morphine concentration favors the wild-type virus regardless of other parameter values. Since some mutant virus is always produced from the wild-type, this makes CE the stable equilibrium. The MOE is stabilized by low morphine, a low fitness cost, and high chance of immune escape. At a sufficiently lower morphine concentration, high fitness cost and low escape ratio result in a stable IFE, thereby controlling the infection.

3.4. Effects of morphine on virus-cell dynamics: Model simulations

We now present the model simulations to observe the effects of morphine on the virus-cell dynamics. Since $R_0 > 1$ for our base parameter values, we expect that the infection is established for any concentrations of morphine, as revealed in the simulations (Figure 6a). We found $\sim$1.5 $\log_{10}$ increase in set-point viral load (Figure 6a) and $\sim$300 count decrease in CD4 (Figure 6b) for the morphine conditioning of $M = 200$ compared to the absence of morphine ($M = 0$), consistent

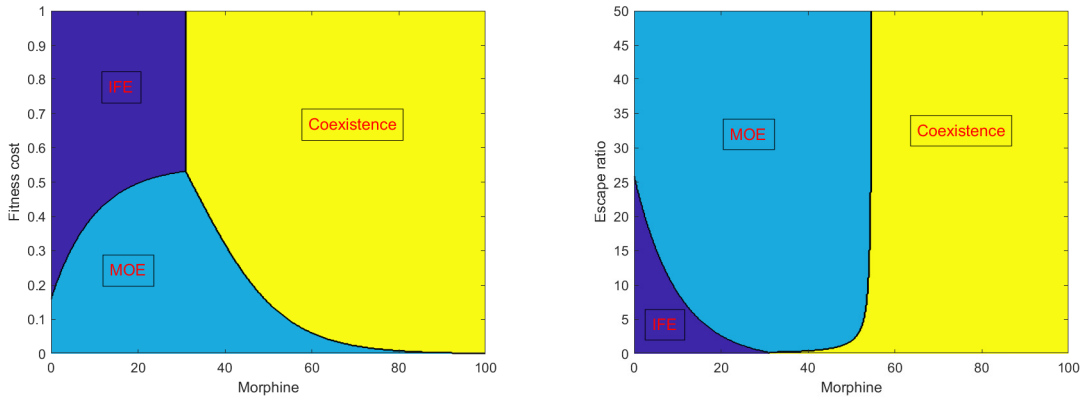

Figure 5: Model predicted stability regions for Infection-Free Equilibirum (dark-blue), Mutant-Only Equilibrium (light-blue) and Coexistence Equilibirum (yellow) in $M - F$ space (left, with $B = 30$) and $M - B$ space (right, with $F = 0.1$).

with the experimental results [6].

We also present the dynamics of wild-type and mutant virus in the absence ($M = 0$, Figure 6c) and presence ($M = 200$, Figure 6d) of morphine. For $M = 0$, the mutant virus quickly out-competes with the wild-type, and in the long run, the viral load consists entirely of the mutant population, with the wild-type population going extinct (Figure 6c). If excessive morphine is in the system, i.e., $M = 200$, both virus species co-exist, with the wild-type population dominating the mutant population (Figure 6d).

To investigate the altered viral dynamics due to the presence of morphine on the effectiveness of antiretroviral therapy (ART), we introduced ART via reverse transcriptase and protease inhibition [49]. These drugs can be introduced into our model by performing the following transformations: $\beta_i \to (1 - \Phi)\beta_i, i = l, h$ (reverse transcriptase inhibitors), and $p \to (1 - \Psi)p$ (protease inhibitors), where Φ and Ψ are efficacy of corresponding ARTs. In Figure 7, we present simulations of a course of ARTs with 90% efficacy initiated at the steady state. In Figure 7 (left), we present the viral dynamics in the absence and presence of morphine both before and after ART treatment. We observed that the combined morphine effects in our model caused 7 days longer for the viral load to reach the detection limit (50 viral RNA copies per ml) (Figure 7 left). In Figure 7 (right), we first simulate the viral dynamics until a steady state with M = 200 (presence of morphine). Once a steady state is reached, we began ART under two conditions: one without morphine (M=0) and

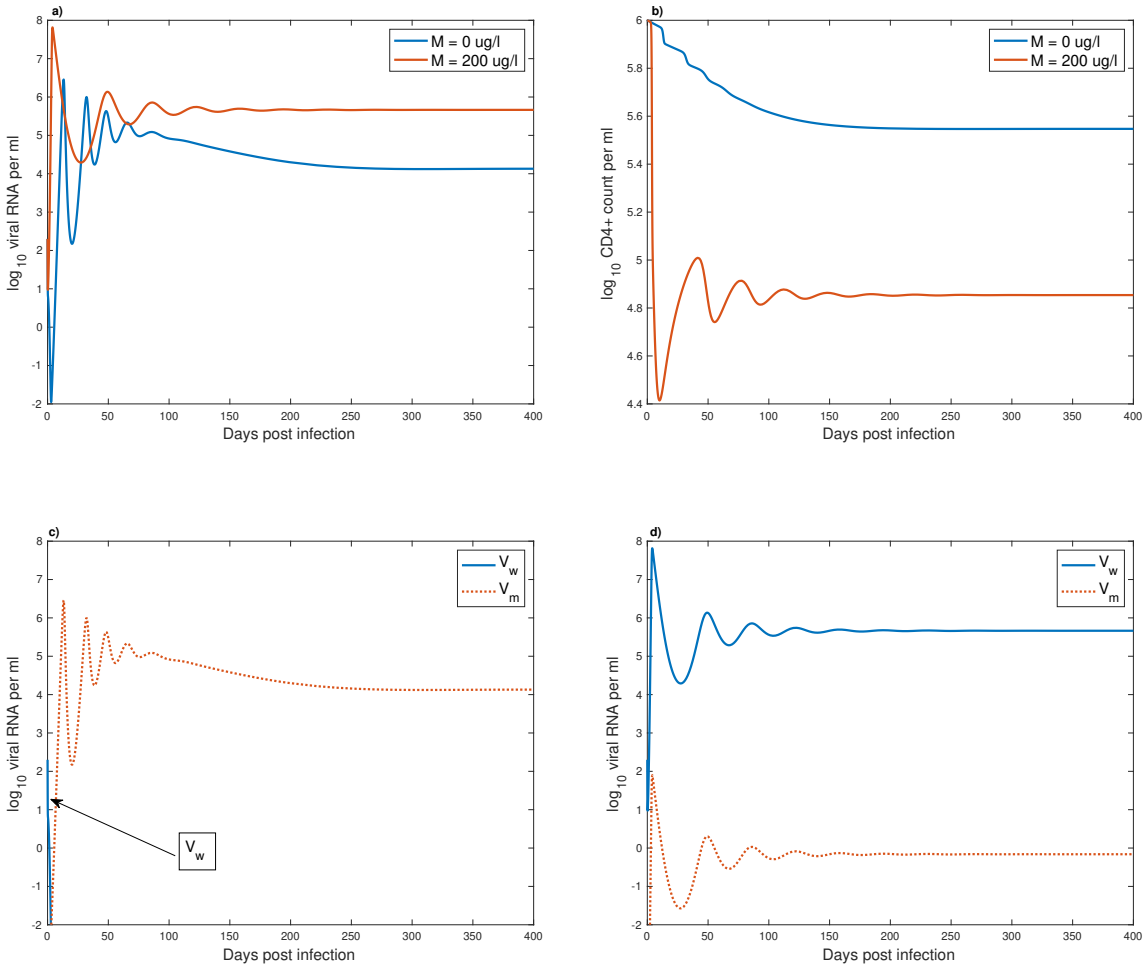

Figure 6: (a) Model predicted viral load and (b) CD4+ count for 400 days post-infection for absence ($M = 0$) and presence ($M = 200$) of morphine. Dynamics of the wild-type and mutant virus populations in (c) the absence ($M = 0$) and (d) the presence ($M = 200$) of morphine.

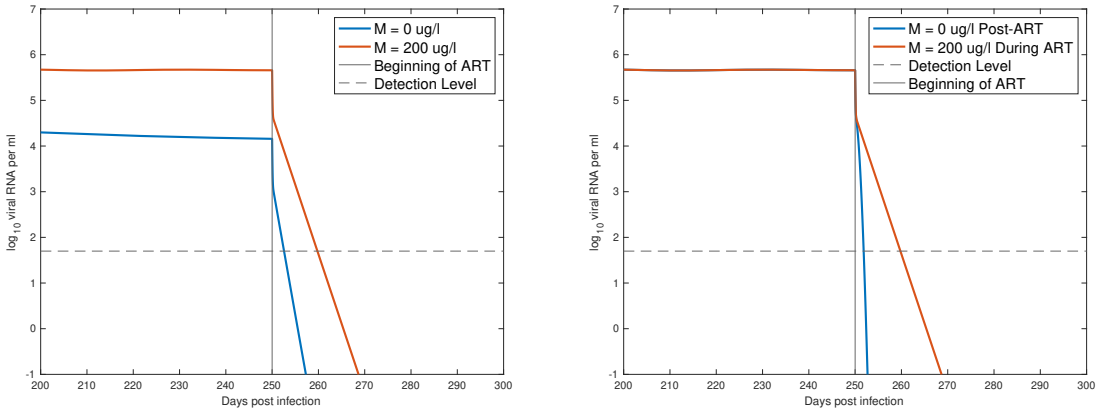

Figure 7: Model simulation of a course of antiretroviral therapy. (Left) ART was started after the model was allowed to come to steady state. When morphine is not being used (blue), the model predicts a 2 day lag for the virus to become undetectable versus 9 days when morphine is being used (red). (Right) After reaching the steady state under morphine conditioning, ART was initiated with two conditions: one in the absence of post-ART morphine (blue) and another in the presence of post-ART morphine (red).

another with M = 200. These two conditions represent the first patient who stops taking drugs of abuse once ART begins and the second patient who continues taking drugs of abuse even after ART. This result (Figure 7 (right)) further confirms that the viral load falls below the detection limit faster when morphine is not present.

3.5. Sensitivity of viral load and CD4+ count

Here we investigate the sensitivity of set-point viral load and CD4+ count to parameter changes under various morphine concentrations. For each parameter ρ, 10,000 values were sampled via LHS from an interval $[\rho_{min}, \rho_{max}]$ with lower- and upper-bounds chosen to give a wide range of biologically-relevant values (Table 1). After sampling, PRCCs were computed as the Pearson correlation coefficient between the model output and sampled parameter values [44].

Figure 8 (a) and (b) show the PRCCs between the parameters and set-point viral loads for $M = 0$ and $M = 200$, respectively. Similarly, Figure 8 (c) and (d) show the PRCCs between parameters and CD4+ counts for $M = 0$ and $M = 200$, respectively. Total viral load and CD4+ are both positively associated with target cell recruitment λ. Viral load is positively associated with virus production p and negatively associated with the death parameters δ_T and δ_V. CD4+

counts are most negatively associated with the transition rate r and positively associated with viral clearance δ_V.

In the absence of morphine (Figure 8a), the total viral load is more sensitive to the fitness cost F because the mutant virus is dominant, and a higher fitness cost corresponds to a weaker virus. When morphine is in use (Figure 8b), the infected cell death rate δ_I had a higher global sensitivity as well. Similarly, in the absence of morphine (Figure 8c), CD4+ counts were more sensitive to F as well as to CTL-related parameters b, ω, and δ_C compared to the high morphine case (Figure 8d). This is expected since the lower morphine case has a stronger response by CTLs and those parameters have a larger effect.

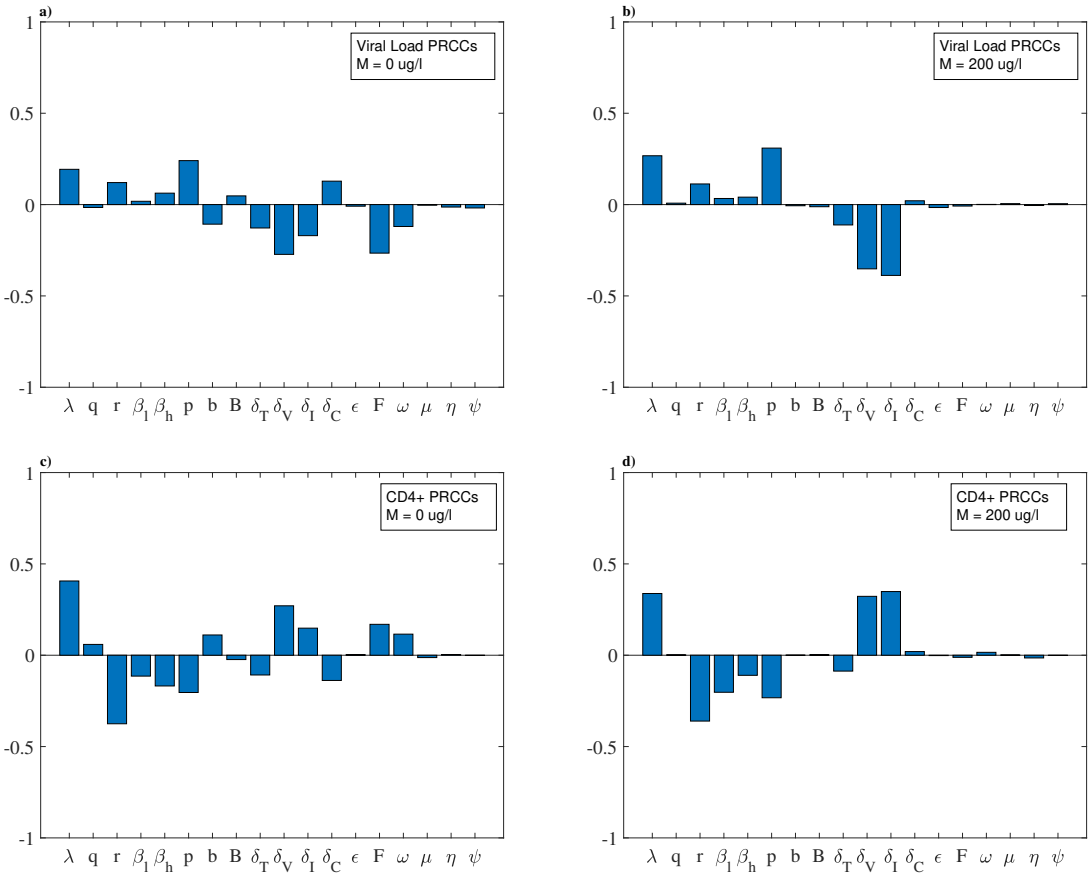

Figure 8: The partial rank correlation coefficients obtained from Latin hypercube sampling method for set-point viral load (a,b) and CD4+ count (c,d) in the absence ($M = 0$) and in the presence ($M = 200$) of morphine.

4. Conclusion

HIV is an ongoing public health problem worldwide, and the recreational use of injection drugs is one of the main risk factors for contracting it [2]. In addition to increasing the risk of contracting HIV, injection drug use has been shown to have several adverse effects, such as a faster progression to AIDS, a higher chance of HIV-related neurological complications, increased set-point viral load, and decreased immune response [6, 7]. In this study, we developed a mathematical model of HIV dynamics to investigate the effect of drugs of abuse (morphine) on viral load, immune responses, and viral mutation. This model expands on previous models of HIV wild-type-mutant dynamics with the inclusion of morphine-affected mechanisms [19, 50]. We analyzed our model to determine the short- and long-term outcome of an HIV infection in the presence of drugs of abuse.

We identified three biologically-relevant equilibria of our model and characterized their stability in terms of the morphine level present in the system, the fitness cost of mutation of the virus, and the viral escape ratio. Using numerical techniques, we were able to identify the threshold morphine concentration that determines whether the wild-type or mutant virus dominates, M_{thresh}. We also found $\sim$1.5 $\log_{10}$ increase in set-point viral load and $\sim$300 count decrease in CD4 when morphine was present in the body of an infected host.

Since morphine inhibits CTL responses, our model predicted a higher set-point viral load in the presence of morphine. Notably, our model showed that wild-type virus dominates in morphine conditioning due to a diminished viral mutation caused by morphine. We also found that a low fitness cost and high escape ratio lead to a state where the wild-type virus goes extinct as the mutant virus out-competes, and the virus population is entirely mutant (the mutant-only equilibrium). On the other hand, high morphine gives an advantage to the wild-type virus, increasing the total viral load with the wild-type virus dominating.

Several clinically relevant insights can be gleaned from our model. Our model prediction related to competition dynamics of two viral species influenced by drug use has not been studied experimentally; the results in this paper may motivate such clinical work. A longer time for viral suppression due to ART treatment for morphine conditioning provides important implications for designing treatment protocols for drug-addicted individuals. Other modeling studies with wild-type and mutant viruses have investigated treatment strategies when the mutant is resistant to ART [50]. One of the bases of our model presented here is the decrease in viral mutation due to morphine [21, 22]. Our modeling results can also be relevant to the potential reduction of the emergence

of ART resistance in the drug-addicted group, thereby providing useful information for successful treatment strategies for drug abusers.

Our model has several limitations. The body metabolizes morphine, and its concentration decreases over time [41]. We assumed a constant morphine concentration, M, and used this value in the analysis of the model. Future work should include time-dependent concentrations using the pharmacokinetics of morphine. Additionally, long-term infection dynamics may be impacted by antibody responses and the presence of latently infected cells [28, 31]. Including these factors in the model may improve our understanding of viral dynamics and mutation under morphine conditioning. Based on previous studies on HIV, we only considered the fitness cost of mutation. If there is a chance that mutation can result in a more fit mutant with an additional advantage over the wild-type, future investigations may need to consider viral mutation with virus species of various fitnesses. Our model assumed the increased viral load under morphine conditioning is only related to morphine use, as adopted in the experiments. However, we acknowledge that more severe diseases could also be due to other factors related to drug use, such as poor diet or lifestyle. Also, further experimental data with frequent measurement of viral loads, virus species populations, and CTLs may help strengthen those effects of morphine introduced into the model.

To summarize, we developed a novel model to investigate the effects of morphine on within-host dynamics of wild-type and mutant HIV species. Our model predicts that the role of morphine in increased susceptibility of the target cells, decreased CTL responses, and decreased mutation eventually results in an increase in set-point viral load and a decrease in CD4 count. We identified three biologically relevant steady-states of our model and characterized them based on morphine concentration, the fitness cost of mutation, and viral escape. Our results may help design proper control measures for HIV infection within drug abusers.

Acknowledgement

This work was funded by NSF grants DMS-1951793, DMS-1836647, and DMS-1616299 from National Science Foundation, the United States, and the UGP award and the start-up fund (NKV) from San Diego State University. The funders had no role in study design, data collection, analysis, decision to publish, or manuscript preparation.

References

[1] UNAIDS. UNAIDS Data 2021 (2021).

[2] Alcabes, P.; Friedland, G. Injection drug use and human Immunodeficiency Virus Infection. *Clin. Infect. Dis.* **1995**, 20, 1467–1479.

[3] Fauci, A. S. Pathogensis of HIV disease: Opportunities for new prevention interventions. *Clin. Infect. Dis.* **2007**, 45, S206-S212.

[4] Kohli, R.; Lo, Y.; Howard, A. A.; Buono, D.; Floris-Moore, M.; Klein, R. S.; Schoenbaum, E. E. Mortality in an Urban Cohort of HIV-Infected and At-Risk Drug Users in the Era of Highly Active Antiretroviral Therapy. *Clin. Infect. Dis.* **2005**, 41, 864-872.

[5] Li, Y.; Wang, X.; Tian, S.; Guo, C.; Douglas, S. D.; Ho, W. Methadone enhances human immunodeficiency virus infection of human immune cells. *J. Infect. Dis.* **2002**, 185, 118-122.

[6] Kumar, R.; Torres, C.; Yamamura, Y.; Rodriguez, I.; Martinez, M.; Staprans, S.; Donahoe, R. M.; Kraiselburd, E.; Stephens, E. B.; Kumar, A. Modulation by morphine of viral set point in rhesus macaques infected with simian immunodeficiency virus and simian-human immunodeficiency virus. *J. Virol.* **2004**, 78, 11425-11428.

[7] Hauser, K. F.; Hahn, Y. K.; Adjan, V. V.; Zou, S.; Buch, S. K.; Nath, A.; Bruce-Kelle, A. J.; Knapp, P. E. HIV-1 tat and morphine have interactive effects on oligodendrocyte survival and morphology. *Glia* **2009**, 57, 194-206.

[8] Kitchen, S. G.; Whitmire, J. K.; Jones, N. R.; Galic, Z.; Kitchen, C. M. R.; Ahmed, R.; Zack, J. A.; Chisari, F. V. The CD4 molecule on CD8+ T lymphocytes directly enhances the immune response to viral and cellular anitgens. *Proc. Natl. Acad. Sci. U.S.A.* **2005**, 102, 3794-3799.

[9] Kileen, N.; Davis, C. B.; Chu, K.; Crooks, M. E. C.; Sawada, S.; Scarborough, J. D.; Boyd, K. A.; Stuart, S. G.; Xu, H.; Littman, D. R. CD4 function in thymocyte differentiation and T cell activation. *Philos. Trans. R. Soc. Lond., B, Biol. Sci.* **1993**, 342, 25-34.

[10] Chan, D. C.; Kim, P. S. HIV entry and its inhibition. *Cell.* **1998**, 93, 681-684.

[11] Greenough, T. C.; Brettler, D. B.; Somasundaran, M.; Panicali, D. L.; Sullivan, J. L. Human immunodeficiency virus type 1- specific cytotoxic T lymphocytes (CTL), virus load, and CD4 T cell loss: evidence supporting a protective role for CTL in vivo. *J. Infect. Dis.* **1997**, 176, 118-125.

[12] Ganusov, V. V.; Neher, R. A.; Perelson, A. S. Mathematical modeling of escape of HIV from cytotoxic T lymphocyte responses. *J. Stat. Mech.* **2013**, 2013, P01010-P01010.

[13] Klein, M. R.; van der Burg, S. H.; Pontesilli, O.; Miedema, F. Cytotoxic T lymphocytes in HIV-1 infection: a killing paradox? *Immun. Today* **1998**, 19, 317-324.

[14] Fryer, H. R.; Frater, J.; Duda, A.; Roberts, M.G.; SPARTAC Trial Inverstigators; Phillips, R. E.; McLean, A. R. Modelling the Evolution and Spread of HIV Immune Escape Mutants. *PloS Pathogens* **2010**, 6.

[15] Ribeiro, R. M.; Chavez, L. L.; Li, D.; Self, S. G.;Perelson, A. S. Estimation of the initial viral growth rate and basic reproductive number during acute HIV-1 infection. *J. Virol.* **2010**, 84, 6096-6102.

[16] Boutwell, C. L.; Rolland, M. M.; Herbeck, J. T.; Mullins, J. I.; Allen, T. M. Viral evolutions and escape during acute HIV-1 infection. *J. Infect. Dis.* **2010**, 202, S309-S314.

[17] McMichael A. J.; Rowland-Jones, S. L. Cellular immune responses to HIV. *Nature* **2001**, 410, 980-987.

[18] Deng, L.; Pertea, M.; Rongvauz, A.; Want, L.; Durand, C. M.; Ghiaur, G.; Lai, J.; McHugh, H. L.; Hao, H.; Margolick, J. B.; Gurer, C.; Murphy, A. J.; Valenzuela, D. M.; Yancopoulus, G. D.; Deeks, S. G.; Stowig, T.; Kumar, P.; Siliciano, J. D.; Salzberg, S. L.; Flavell, R. A.; Shan, L.; Siliciano, R. F. Broad CTL response is required to clear latent HIV-1 due to dominance of escape mutations. *Nature* **2015**, 381-385.

[19] Konrad, B. P.; Vaiyda, N. K.; Smith?, R. J. Modeling mutation to a cytotoxic T-lymphocyte HIV vaccine. *Math. Popul. Stud.* **2011**, 18, 122-149.

[20] Barouch, D. H.; Kunstman, J.; Glowczwskie, J.; Kunstman, K. J.; Egan, M. A.; Peyerl, F. W.; Santra, S.; Kuroda, M. J.; Schmitz, J. E.; Beaudry, K.; Krivulka, G. R.; Lifton, M. A.; Gorgon, D. A.; Wolinsky, S. M.; Letvin, N. L. Viral escape from dominant simian immunodeficiency virus epitope-specific cytotoxic T lymphocytes in DNA-caccinated rhesus monkeys. *J. Virol.* **2003**, 77, 7367-7375.

[21] Noel, R.; Marrero-Otero, Z.; Kumar, R.; Chompre-Gonzalez, G. S.; Verma, A. S.; Kumar, A. Correlation between SIV tat evolution and AIDS progression in cerebrospinal fluid of morphine-dependent and control macaques infected with SIV and SHIV. *Virology* **2006**, 349, 440-452.

[22] Noel, R.; Kumar, A. SIV vpr evolution is inversely related to disease progression in a morphine-dependent rhesus macaque model of AIDS. *Virology* **2007**, 359, 397-404.

[23] Rivera-Amill, V.; Silverstein, P. S.; Noel, R.; Kumar, S.; Kumar, A. Morphine and rapid disease progression in nonhuman primate model of AIDS: Inverse correlation between disease

progression and virus evolution. *J. Neuroimmune Pharmacol* **2014**, 5, 122-132.

[24] Fuggetta, M.P.; Di Francesco, P.; Falchetti. R.; Cottarelli, A.; Rossi, L.; Tricarico, M.; Lanzilli, G. Effect of morphine on cell-mediated immune responses of human lymphocytes against allogeneic malignant cells. *J Exp Clin Cancer Res* **2005**, 24(2), 255-63.

[25] Miyagi, T.; Chuang, L. F.; Doi, R. H.; Carlos, M. P.; Torres, J. V.; Chuang R. Y. Morphine induces gene expression of antiviral CCR5 in human CEMx174 lymphocytes. *J. Biol. Chem.* **2010**, 275, 31305-31310.

[26] Perelson, A. S.; Ribeiro, R. M. Modeling the within-host dynamics of HIV infection. *BMC Biol.* **2013**, 11.

[27] Chubb M. C.; Jacobsen, K. H. Mathematical modeling and the epidemiological research process. *Eur. J. Epidemiol.* **2010**, 25, 13-19.

[28] Conway, J. M.; Perelson, A. S. Post-treatment control of HIV infection. *PNAS,* **2015**, 112, 5467-5472.

[29] Schwartz, E. S.; Biggs, K. R. H.; Bailes, C.; Ferolito, K. A.; Vaidya, N. K. HIV dynamics with immune responses: Perspectives from mathematical modeling. *Curr. Clin. Microbiol. Rep.* **2016**, 3, 216-224.

[30] Vaidya, N. K.; Ribeiro, R. M.; Perelson, A. S.; Kumar, A. Modeling the effects of morphine on simian immunodeficiency virus dynamics. *PloS Comput. Biol.* **2016**, 12, e1005127.

[31] Mutua, J. M.; Perelson, A. S.; Kumar, A.; Vaidya, N. K. Modeling the Effects of Morphine Altered Virus Specific Antibody Responses on HIV/SIV Dynamics. *Sci. Rep* **2019**, 9, 5423.

[32] Ganusov, V. V.; De Boer, R. J. Estimating costs and benefits of CTL escape mutations in SIV/HIV infection. *PloS Comput. Biol.* **2006**, 3, e24.

[33] Ganusov, V. V.; Goonetilleke, N.; Liu, M. K. P.; Ferrari, G.; Shaw, G. M.; McMichael, A. J.; Borrow, P.; Korber, B. T.; Perelson, A. S. Fitness Costs and Diversity of the Cytotoxic T Lymphocyte (CTL) Response Determine the Rate of CTL Escape during Acute and Chronic Phases of HIV Infection. *J. Virol.* **2011**, 85, 10518-10528.

[34] De Boer, R. J.; Perelson, A. S. Target cell limited and immune control models of HIV jnfection: A comparison. *J. Theor. Biol.* **1998**, 190, 201-214.

[35] Vaidya, N.K.; Peter, M. Modeling Intracellular Delay in Within-Host HIV Dynamics Under Conditioning of Drugs of Abuse. *Bull. Math. Biol.* **2021** 83, 81.

[36] Stafford, M. A.; Corey, L.; Cao, Y.; Daar, E. S.; Ho, D. D.; Perelson, A. S. Modeling plasma

virus concentration during primary HIV infection. *J. Theor. Biol.* **2000**, 203, 285-301.

[37] Ramratnam, B.; Bonhoeffer, S.; Binley, J.; Hurley, A.; Zhang, L.; Mittler, J. E.; Markowitz, M.; Moore, J. P.; Perelson, A. S.; Ho, D. D. Rapid production and clearance of HIV-1 and hepatitis C virus assessed by large volume plasma apheresis. *Lancet.* **1999**, 354, 1782.

[38] Mansky, L. M.; Temin, H. M. Lower in vivo mutation rate of human immunodeficiency virus type 1 than that predicted from the fidelity of purified reverse transcriptase. *J. Virol.* **1995**, 69, 5087-5094.

[39] Adams, B. M.; Banks, H. T.; Davidian, M.; Kwon, H.-D.; Tran, H. T.; Wynne, S. N. and Rosenberg, E. S. HIV dynamics: Modeling, data analysis, and optimal treatment protocols. *J. Comput. Appl. Math.* **2005**, 184(1): 10-49.

[40] Tarfulea, N. E. A mathematical model for CTL effect on a latently infected cell inclusive HIV dynamics and treatment. *AIP Conf. Proc.* **2017** 1895(1): 070005.

[41] Olkkola, K. T.; Maunuksela, E.; Korpela, R.; Rosenberg, P. H. Kinetics and dynamics of postoperative intravenous morphine in children. *Clin. Pharmacol. Ther.* **1988**, 44, 128-136.

[42] Castillo-Chavez, C.; Feng, Z.; Huang, W. *Mathematical Approaches for Emerging and Reemerging Infections Diseases: An Introduction,* 1st ed.; Springer-Verlag, New York, 2002, pp. 229-250.

[43] Diekmann, O.; Heesterbeek, J. A. P.; Roberts, M. G. The construction of next-generation matrices for compartmental epidemic models. *J. R. Soc. Interface* **2009**, 7, 873-875.

[44] Marino, S.; Hogue, I. B.; Ray, C. J.; Kirschner, D. E. A methodology for performing global uncertainty and sensitivity analysis in systems biology. *J. Theor. Biol.* **2008**, 254, 178-196.

[45] Perera, S. D.; Perera, S. S. N.; Jayasinghe, S. Modeling and sensitivity of dengue viral dynamics. *Int. J. Curr. Res.* **2006**, 8, 34899-34906.

[46] Rodrigues, H.S.; Monteiro, M. T. T.; Torres, D. F. M. Sensitivity analysis in a dengue epidemiological model. *Conference Papers in Mathematics* **2013**, 2013, 721406.

[47] Perko, L. *Differential equations and dynamical systems*, 2nd ed.; Springer-Verlag, New York, 1991.

[48] Jordan, D. W.; Smith, P. *Nonlinear ordinary differential equations: An introduction to dynamical systems*, 3rd ed.; Oxford University Press, New York, 1999.

[49] Vaidya, V. K.; Rong, L. Modeling pharmacodynamics on HIV latent infection: Choice of drugs is key to successful cure via early therapy. *SIAM J. Appl. Math.* **2017**, 77, 1781-1804.

[50] Kwon, H.-D. Optimal treatment strategies derived from a HIV model with drug-resistant mutants. *Appl. Math. Comput.* **2007**, 188(2): 1193-1204.

Highlight: “Modeling the Effects of Drugs of Abuse on Within-host Dynamics of Two HIV Species” by *Peter Uhl and Naveen K. Vaidya*

- We develop a mathematical model to study the effects of morphine-altered mutation and cellular immune response on the within-host dynamics of two HIV species, a wild-type and a mutant.
- We establish the condition for mutant virus to out-compete wild-type virus.
- The dominant strain is determined by morphine concentration.
- We identify three biologically relevant equilibria: the infection-free, mutant-only, and coexistence.
- The fitness cost of mutation, mutant escape rate, and morphine concentration characterize the equilibria of the system.

Credit author statement:

Peter Uhl: Modeling, Analysis, Computation, Writing;
Naveen K. Vaidya: Conceptualization and Design, Modeling, Analysis, Supervision, Writing.